[Short title + Author Name - P&H title] 17 (2024) 105799

Contents lists available at ScienceDirect

Arabian Journal of Chemistry

journal homepage: www.ksu.edu.sa

Optoelectronic performance and co-sensitized excited states characteristics of organic dyes with naphthobisthiadiazole and benzothiadiazole

Baishuo Li [a], Jiayu Han [a], Peng Song [b], Yuanzuo Li [a,*]

[a] College of Science, Northeast Forestry University, 150040 Harbin, China
[b] Department of Physics, Liaoning University, Shenyang 110036, Liaoning, China

ARTICLE INFO

Keywords:
Dye-sensitized solar cell
Co-sensitization
Density functional theory
Electron transfer
Organic molecules

ABSTRACT

Photosensitizer systems play a crucial role in light absorption and charge transfer processes. Designing and selecting dye molecules with exceptional photoelectric features remains a significant scientific challenge in the realm of solar cell research. The paper explores the photovoltaic properties of two D-A'-π-A dyes (CS-70 and CS-72) both individually and after co-sensitization with chlorophyll derivatives, utilizing density functional theory (DFT) and time-dependent density-functional theory (TD-DFT) methods. The monomeric dye molecules share the same donor and conjugated bridge but differ in their auxiliary receptors (benzothiadiazole and naphthobisthiadiazole). Firstly, the study investigates the impact of various auxiliary acceptors on the properties of the dye molecules by analyzing their geometrical structure, frontier molecular orbitals, spectral properties, chemical reaction parameters, intramolecular charge transfer, electron injection, density of projected states, and dye regeneration. A detailed explanation for the superior performance of CS-72 is provided. Furthermore, a solar cell evaluation model was developed for the short circuit current density (*Jsc*), open circuit voltage (*Voc*), and photoelectric conversion efficiency (*PCE*) of the single dye molecule. Subsequently, simulations of the co-sensitized molecules with chlorophyll are performed, focusing on structure, excited state properties and charge transfer, suggesting that co-sensitization enhances spectral properties, light-trapping, and regeneration abilities, and long-range charge transfer between the dye molecules and chlorophyll can be found. The results also demonstrate that the *Jsc* of the co-sensitized molecules were improved, which facilitates the realization of a higher *PCE*. This study provides theoretical support for the potential of co-sensitizing dye molecules with chlorophyll to enhance solar cell efficiency, offering valuable insights for the future development of green, cost-effective, and efficient solar cells.

1. Introduction

With the rapid development of industrial society, traditional fossil energy sources are facing depletion and are gradually failing to meet the enormous needs of human society. The emergence of renewable energy has injected a new impetus for social development. Photovoltaic technology has garnered widespread attention among renewable energy sources due to its environmentally friendly and abundant resources. Dye-sensitized solar cells (DSSCs), as the third generation of solar cells, have been extensively studied by numerous countries and have experienced significant advancements due to their relatively simple manufacturing process and high transparency (Grifoni et al., 2021; Barjasteh-Askari et al., 2021, Housecroft and Constable, 2022; Wazzan, 2022). In 1991, O'Regan and Grätzel invented the first DSSC based on organic dyes and nanofilm materials, which achieved an efficiency of 7.1 % (O'Regan and Grätzel, 1991). Subsequently, many researchers have dedicated their efforts to improving its efficiency. DSSCs have five components: conductive glass, nano-TiO_2 porous film, dye sensitizer, redox electrolyte, and counter electrode. Its working principle can be divided into four stages: light absorption, electron injection, electron transfer, and electron harvesting (Ramesh and Gnanavel, 2021; Alizadeh et al., 2022; Elkabous and Karzazi, 2024). Among these stages, the choice of dye sensitizer determines the optical response of the DSSC. It triggers the main steps of photon absorption and the subsequent electron transfer process, playing a crucial role in the cell's working mechanism (Zhang et al., 2020a; Quang et al., 2021; Dolatabadi et al., 2022b).

The D-π-A structure, commonly found in organic dye molecules, facilitates electron transfer from the donor (D) to the acceptor (A) through

* Corresponding author.
E-mail address: yzli@nefu.edu.cn (Y. Li).

https://doi.org/10.1016/j.arabjc.2024.105799
Received 13 January 2024; Accepted 15 April 2024
Available online 16 April 2024

a conjugated π-bridge (π) during photoexcitation; electrons are injected into the conduction band (CB) after these molecules adsorbed onto a TiO_2 film. This structure offers advantages such as easy design, simple synthesis, and a wide range of possible structures (Noh et al., 2021; Bronskaya et al., 2023; Li et al., 2024a). Researchers have been continuously synthesizing new molecules based on this structure. Mohamed et al. recently synthesized metal-free D-π-A dyes using triphenylamine and carbazole as the donors, exploring the effect of different acceptors on dye performance, and the dye with cynoacrylic acid as the acceptor exhibited the highest efficiency of 8.81 % (Elmorsy et al., 2023). Tong et al. synthesized three dyes with medium bandgaps by altering the π-bridges on either side of benzothiadiazole: an irregular PClBDT-TBT, regular PClBDT-BT, and PClBDT-DTBT. The irregular PClBDT-TBT dye effectively inhibited dye aggregation and increased the charge transfer rate, achieving a *PCE* as high as 13.04 % (Tong et al., 2022). Zhou et al. synthesized low-cost D-π-A porphyrins (SGT-021(D0), SGT-021(D)) and an organic dye SGT-149(D), with easily synthesized donor units. SGT-021(D) displayed the best performance with significantly higher open-circuit voltage and a *PCE* of 11.1 % compared to the original dye. This work demonstrated the potential of using low-cost donor units to develop efficient DSSCs with high *Voc* (Zhou et al., 2023). In addition to modifying each functional group within the molecule, co-sensitization is also a popular method to improve the performance of the molecules (Zhang et al., 2020b). Zhang et al. synthesized MS4 and MS5 molecules and co-sensitized MS5 with XYb1, resulting in an efficiency increase of 13.5 % (Zhang et al., 2021). Deeksha et al. investigated the co-sensitization of Ru-complexes with organic dyes, which effectively inhibited dye complexation, promoted charge transfer, and increased the *PCE* from 9.07 % to 11 % compared to monomer dyes (Kharkwal et al.,2021). Chlorophyll, a natural and environmentally friendly dye, has been extensively studied in solar cell research due to its chemical stability and excellent visible light absorption properties (Ethirajan et al., 2011; Tamiaki and Kunieda, 2011, Zhang et al., 2019). Sun et al. synthesized a novel organic dye molecule, D-π-A dye, with chlorophyll derivatives to form a binary photosensitizer through ester bonding (Sun et al.,2018). Ye et al. investigated the co-sensitization of chlorophyll derivatives (H_2-Chl-1) and carotenoids (Car). The optimal mass ratio of H_2Chl-1 to Car (10:3) significantly enhanced the photoactive layer's light absorption capacity and electron extraction efficiency in co-sensitized solar cells, resulting in a 40 % increase in *PCE* (Ye et al., 2022).

Recently, Cui et al. conducted experiments to synthesize three organic dyes, CS-70, CS-71, and CS-72, all of which belong to the D-A'-π-A (A' is auxiliary acceptor) type (Cui et al., 2023). Among these dyes, CS-70 and CS-72 exhibited higher *PCE*. To delve deeper into the photovoltaic properties, we conducted elaborated theoretical calculations on these two molecules. Here, we investigated various aspects of these molecules using DFT and TD-DFT, including their geometries, frontier molecular orbitals (FMOs), absorption spectra, excitation and fluorescence lifetimes, chemical reaction parameters, intramolecular charge transfer, electron injection, dye regeneration, and partial density of states, to reveal performance differences for two dyes incorporating naphthobisthiadiazole or benzothiadiazole as an auxiliary acceptor. After that, considering that the maximum absorption wavelength of CS-72 with the highest experimental *PCE* is only just over 500 nm (514 nm in the experiment), it is insufficient for the full solar spectrum absorption. Therefore, we explore the method of co-sensitization to broaden the light trapping region and increase the *PCE*. Inspired by Ye et al work, H_2Chl molecules, which experimentally exceed 650 nm, were selected as the co-sensitizer (Ye et al.,2022), and by adding chlorophyll and its derivatives as co-sensitizers with strong absorption abilities, the light absorption range is hoped to be widened. The intermolecular interaction mechanism, spectral improvement characteristics, intermolecular long-distance charge transfer, and the effect on the *PCE* of DSSCs after the co-sensitization of CS-series dyes with H_2Chl is not yet very clear. Therefore, we take the two types of molecules as an example and aim to provide a detailed analysis of the performance differences between solar cells using chlorophyll derivatives as co-sensitizers compared to those using single dye molecules as photosensitizers. By investigating the chemical stability, spectral improvement, and charge transfer mechanisms of co-sensitized molecular models, we hope to pave the way for utilizing natural pigments like chlorophyll in enhancing solar cell efficiency. Through this comprehensive study, we provide a theoretical basis for future advancements in solar cell technology.

2. Computation details

All theoretical calculations were performed using the Gaussian 09 software package (Frisch et al., 2009). The ground state properties of the dye molecules were studied by DFT (Parr et al., 1978), and then the excited state properties of the molecules were analyzed by TD-DFT (Runge and Gross, 1984). The ground states of all the monomeric dye molecules were optimized using the B3LYP functional and the 6-31G(d) basis set (Meenakshi, 2017). From these optimized structures, we investigated their geometries, FMOs energy and distributions, ionization potential (IP), electron affinity (EA), electrostatic potentials (ESP), electron injection driving force (ΔG^{inject}), and regeneration driving force (ΔG_{reg}). Considering the presence of weak interactions in the co-sensitized molecules, B3LYP-D3(BJ) was used for optimization (Lu and Chen, 2013). The UV–visible absorption spectrum was determined through TD-DFT using the CAM-B3LYP/6-311G(d, p) method (Suramitr et al., 2012; Roy et al., 2019). Subsequently, CAM-B3LYP/6-31G(d) was used to optimize the dye molecule in the first excited state (Adamo and Jacquemin, 2013). With the optimized model, fluorescence spectra were calculated using TD-DFT/CAM-B3LYP/6-311G(d, p). Also, some properties were calculated, including the excited state lifetime, fluorescence lifetime, light-harvesting efficiency (LHE), and charge transfer. Two solvent models, IEFPCM and SMD, were used to simulate chloroform solvents. The choice of these models was based on the following reasons: the SMD solvent model has a better functional form, especially for the non-polar part (Marenich et al.,2009), but for some systems, especially flexible ones, it may cause difficulties in convergence during optimization, and even result in false frequencies. Therefore, the IEFPCM solvent model was used for geometry optimization (Ren and Li, 2013), while the SMD solvent model was used to calculate single-point energy, UV–vis absorption, fluorescence spectra, interaction energy, and so on. Furthermore, to deeply investigate the photovoltaic performance of the dye@TiO_2 composite system, the 6-31G(d) basis set was used for C, H, O, N, and S atoms, while the LANL2DZ basis set was used for Ti atoms of the ground state optimization (Prakash et al., 2019). The FMOs energy levels and absorption spectrum were plotted using Origin software. In addition, electron excitation diagrams and electrostatic potential diagrams were drawn using VMD software (Koeppe et al., 2007, Pelzer and Darlin, 2016. The charge density difference (CDD) was investigated using the Multiwfn3.8 program to reflect electron transfer and injection (Lu and Chen, 2012, Zang et al., 2023; Zang et al., 2024), while partial density of states (PDOS) in GaussSum was used to analyze the CB edge shifts caused by the molecules (Nagarajan et al., 2017).

PCE is a decisive factor in considering the performance of the dye molecule. The factors affecting the *PCE* are *Voc*, *Jsc*, fill factor (*FF*), and incident light intensity (P_{in}). The following formula can calculate the *PCE* (Kabir and Sakib, 2019):

$$PCE = \frac{J_{SC} V_{OC} FF}{P_{in}} \tag{1}$$

J_{SC} can be calculated from the following equation (Pounraj et al., 2018; Gao et al., 2019):

$$J_{sc} = e \int LHE(\lambda) \Phi_{inj} \eta_{coll} I_S(\lambda) d\lambda \tag{2}$$

$$LHE(\lambda) = 1 - 10^{-\Gamma \sigma(\lambda)} \tag{3}$$

$$\sigma(\lambda) = \varepsilon(\lambda) \times 10^3 \quad (4)$$

Where LHE (λ) denotes the light-harvesting efficiency in the absorption spectral range of dye molecules under the standard Air Mass 1.5 Global (AM 1.5G) solar spectrum, and Γ is the molecular adsorption value (mol·cm^{-2}) on the semiconductor surface (According to experimental values, the CS-70 is 5.5 × 10^{-7} mol·cm^{-2} and the CS-72 is 4.9 × 10^{-7} mol·cm^{-2}. Considering that the volume of H_2Chl is similar to that of the CS-series dyes, the loading amounts of the two co-sensitization systems are the same as those of the monomeric dye molecules), and σ(λ) depends on the molar extinction coefficient (cm^2·mol^{-1}), and Φ_{inj} and η_{coll} denote the electron injection and collection efficiencies. According to Islam et al., we consider that ideal condition that, all molecular Φ_{inj} tends to 1. In practical experiments, the photoanode and counter electrode are the same; therefore, the molecular collection efficiency (η_{coll}) can be assumed to be the same. Here, we consider the ideal state and define η_{coll} as 1.

Voc can be calculated from the following equation (Arslan et al.,2019):

$$Voc = \frac{E_{CB} + \Delta E_{CB}}{e} + \frac{K_B T}{e} ln\left(\frac{n_c}{N_{CB}}\right) - \frac{E_{redox}}{e} \quad (5)$$

Where ΔE_{CB} is the side shift of the CB of TiO_2, and *e* is the value of the *meta*-charge, and n_c is the number of electrons in the TiO_2 conduction band, and N_{CB} is the number of electrons in the active density state of the TiO_2 conduction band, and E_{redox} is the potential value of the redox pair. The *Voc* is defined as the potential difference between the redox potential of the electrolyte in titanium dioxide and the Fermi energy level. It can be found that ΔE_{CB} and the number of conduction band electrons are the key factors in determining *Voc*. The formula for ΔE_{CB} is as follows (Lee and Yoon, 2018):

$$\Delta E_{CB} = \frac{-e\mu_{normal}\gamma}{\varepsilon\varepsilon_0} \quad (6)$$

Where μ_{normal} is the dipole moment in molecular space, and γ describes the concentration of the dye, and ε and ε_0 denote the vacuum permittivity and relative permittivity of the medium.

3. Results and discussion

3.1. Molecular geometry

It is well known that incorporating suitable groups with strong electron-absorbing ability as auxiliary acceptors between the donor and conjugated π-bridges of the dye molecule can effectively enhance the dye's photostability and power conversion efficiency (Wu et al., 2020). The donor part of studying molecules is a triphenylamine derivative, and the auxiliary acceptors are benzothiadiazole and naphthobisthiadiazole, respectively. Fig. 1 shows the structural features of two optimized D-A´-π-A dyes. Their bond lengths and dihedral angles are listed in Table S1. It can be seen that both molecules have similar twisting features of α_1 (between donor and auxiliary acceptor) and α_2 (between auxiliary acceptor and π-bridge). However, the angle of CS-72 is slightly larger than that of CS-70, which may inhibit dye aggregation (An et al., 2021). The dihedral angles between the donor and auxiliary acceptor of the two molecules (33.03°, 34.45°) are in good agreement with the calculated results (32.9°, 34.8°), which reflects the accuracy of the simulated structures. The α_3 (between the π-bridge and the acceptor) of the two molecules are −0.17° and 0.15°, respectively, which are almost planar structures, favoring electron transfer into semiconductor (Zhang et al., 2013). In addition, the bond lengths of the two molecules did not differ significantly, with both d_1-d_3 ranging from 1.47-1.49 Å, suggesting that the dye molecule has a stable structure (Johnson et al., 2010; Hachi et al., 2021).

3.2. Frontline molecular orbital

The highest occupied molecular orbital (HOMO) and the lowest unoccupied molecular orbital (LUMO) are important parameters for measuring molecular performance. To ensure that the dye molecules have efficient electron injection and regeneration process, the HOMO energy should be lower than the redox potential of the I^-/I_3^- electron pair, and the LUMO energy should be higher than the E_{CB} of TiO_2 (Lazrak et al., 2018; Sharma et al., 2018). And a lower energy gap facilitates easier electronic excitation and makes the absorption spectra red-shifted (Sen and Groβ, 2020). For this purpose, the HOMO, LUMO, and energy gap values of these molecules were calculated and displayed in Fig. 2. The HOMO of the two molecules (−4.82 eV, −4.85 eV) are approximately equal and below the redox potential of I^-/I_3^- (−4.60 eV), and this suggests that electrons can be rapidly transferred from the electrolyte

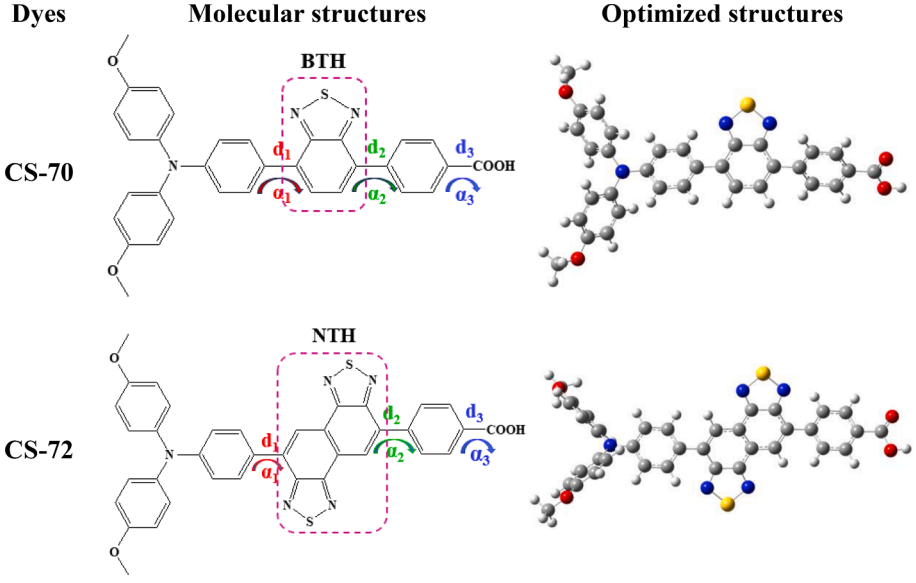

Fig. 1. Molecular structures and ground state optimization structures of CS-70 and CS-72.

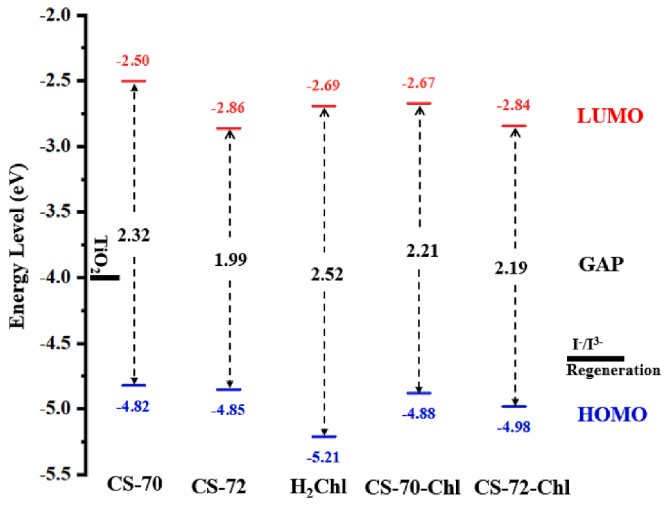

Fig. 2. Energy levels diagram and values of the energy gap of all isolated and dimer.

solution to the oxidized dye for dye regeneration. The LUMO of two molecules (−2.50 eV, −2.86 eV) is much higher than that of the E_{CB} of TiO_2 (−4.00 eV), suggesting that the dye in the excited state can efficiently inject electrons into the CB of TiO_2. In addition, the LUMO of CS-72 (−2.86 eV) is significantly lower than that of CS-70 (−2.50 eV), which suggests that the introduction of naphthobisthiadiazole achieves the selective optimization of the energy level and improve energy gaps and spectra. This can effectively improve the photovoltaic performance of dye molecules. For the energy gap, the energy gap of CS-72 is also significantly reduced compared with that of CS-70 due to the reduction of the LUMO energy level from the introduction of naphthobisthiadiazole, which is favorable to induce CS-72 to absorb longer wavelengths of sunlight. Meanwhile, the theoretical calculations are consistent with the experimental trends, which verifies the reliability of the theoretical calculations.

To delve into the distribution of HOMO and LUMO orbitals, Fig. 3 illustrates the FMOs distribution maps. The contribution of each fragment (donor, auxiliary acceptor, and benzoic acid) to the orbitals of the two molecules is quantitatively depicted in Fig. S1. The HOMOs of CS-70 and CS-72 are predominantly located in the donor portion (90.2 %, 90.2 %) with a minor presence in the auxiliary acceptor (8.1 %, 8.9 %). In contrast, the LUMO is mainly situated in the auxiliary acceptor (82.0 %, 88.5 %) and benzoic acid (10.7 %, 6.2 %). The transfer phenomenon from HOMO to LUMO in both molecules indicates strong intramolecular charge transfer (ICT) properties. Moreover, the higher percentage contribution of naphthobisthiadiazole (88.5 %) to the LUMO compared to benzothiadiazole (82.0 %) suggests a greater electron absorption capacity. Interaction with titanium dioxide results in the HOMO primarily localized on the donor molecule, while the LUMO was distributed onto the titanium dioxide, enhancing ICT phenomenon.

3.3. *Properties of absorption and fluorescence spectra*

UV–Vis absorption and fluorescence spectra are important parameters for measuring the photovoltaic properties of molecules. The excitation properties of the S1-S6 states of the molecule were calculated, including the vertical excitation energy (E), oscillator strength (f), absorption wavelength (λ), major transition modes, and those related parameters are listed in Table 1. The UV–visible absorption spectra are also shown in Fig. 4. As illustrated, both CS-70 and CS-72 exhibit two primary absorption peaks; the short-wavelength absorption range falls within 250–330 nm and 270–350 nm for two dyes, with absorption

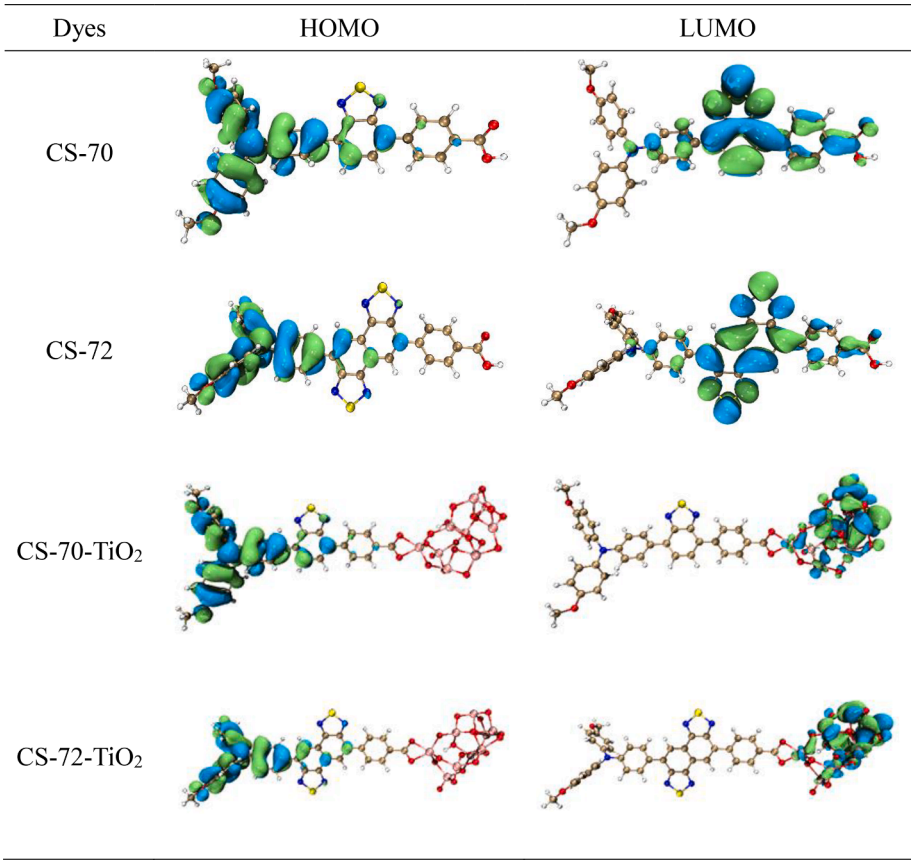

Fig. 3. The frontier molecular orbitals (FMOs) diagram.

Table 1
The calculation of excitation energy (E in eV), absorption wavelength (λ in nm), oscillator strength (f), and main electronic transition configuration of dyes.

Dyes	State	E(eV)	λ(nm)	f	Transition mode
CS-70	1	2.806	441.84	0.752	H → L(0.62)
	2	3.765	329.30	0.015	H-1 → L(0.58)
	3	4.087	303.37	0.126	H → L + 2(0.52)
	4	4.138	299.60	0.887	H → L + 3(0.42)
	5	4.407	281.37	0.211	H-6 → L(0.57)
	6	4.534	273.45	0.265	H → L + 5(0.65)
CS-72	1	2.554	485.42	0.791	H → L(0.61)
	2	3.375	367.37	0.084	H-1 → L(0.57)
	3	3.709	334.32	0.003	H → L + 1(0.55)
	4	3.917	316.50	0.496	H-4 → L(0.54)
	5	4.076	304.17	1.000	H-4 → L(0.38)
	6	4.112	301.54	0.068	H → L + 4(0.66)
H_2Chl	1	2.049	605.17	0.246	H → L(0.63)
	2	2.385	519.88	0.024	H-1 → L(0.57)
	3	3.140	394.80	1.620	H → L + 1(0.57)
	4	3.273	378.71	1.207	H-1 → L + 1(0.61)
	5	3.709	334.29	0.145	H-2 → L(0.60)
	6	3.827	324.01	0.048	H-3 → L(0.62)
CS-70-Chl	1	2.023	612.81	0.188	H-1 → L(0.63)
	2	2.363	524.69	0.017	H-2 → L0.55)
	3	2.598	477.21	0.552	H → L + 1(0.57)
	4	2.637	470.16	0.002	H-1 → L + 1(0.69)
	5	2.771	447.41	0.008	H → L(0.59)
	6	2.905	426.85	0.125	H-2 → L + 1(0.63)
CS-72-Chl	1	1.991	622.84	0.151	H → L + 1(0.45)
	2	2.257	549.35	0.150	H → L(0.47)
	3	2.386	519.69	0.143	H-2 → L + 1(0.38)
	4	2.462	503.54	0.298	H-1 → L(0.56)
	5	2.628	471.76	0.146	H-2 → L(0.58)
	6	2.923	424.24	0.099	H-1 → L + 1(0.55)

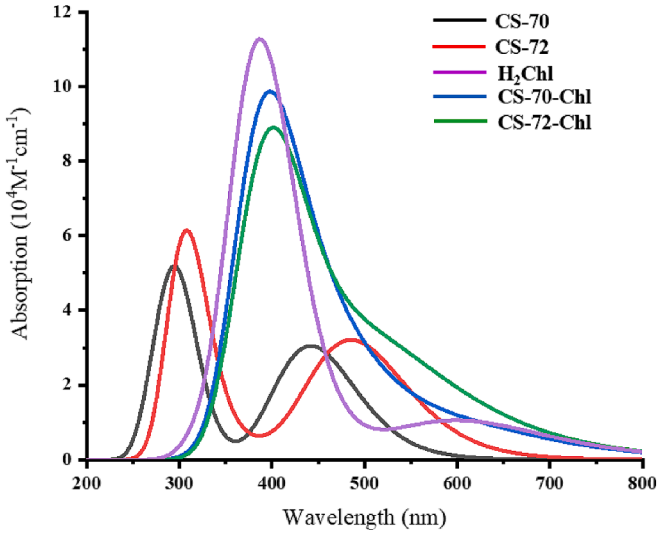

Fig. 4. The simulated UV–vis absorption spectra.

peaks at 299.60 nm and 304.17 nm corresponding to main transition forms of HOMO → LUMO+3 and HOMO-4 → LUMO, respectively. Different from the above excited states, the maximum absorption peaks of the two molecules displayed the main transition mode of HOMO → LUMO. Examination of the orbital diagrams unveils distinctive features such as the nodal surface along the bonding axis in the HOMO, signifying a π orbital, and the anti-bonding traits between C = N and N-S in the LUMO, indicative of a π* orbital. Consequently, both molecules engage in a π → π* transition, recognized as one of the lowest-energy transition forms (Preat et al., 2010). The long-wavelength absorption ranges for CS-70 and CS-72 span 400–500 nm and 425–550 nm, respectively. Notably, due to the more extended conjugation system in CS-72, its maximum absorption wavelength displays a marked redshift to 485.42 nm compared to CS-70′s 441.84 nm, aligning with experimental observations (514 nm of CS-72 is larger than 468 nm of CS-70) (Cui et al., 2023).

The molecules in the first excited state were optimized and the fluorescence spectra were displayed in Fig S2, and the relevant data are displayed in Table 2. The emission wavelengths of CS-70 and CS-72 were 567.71 nm and 602.05 nm, with a distinct red-shifted trend compared to the absorption spectra (125.87 nm and 116.63 nm, respectively). This indicates that the two dye molecules have good immunity to interference in the optoelectronic material system (Choudhary et al., 2013). In addition, the dye molecules' excited state lifetimes and fluorescence lifetimes were calculated, and long excited state lifetimes will provide sufficient time for electron injection (Le Bahers et al.,2009). The fluorescence lifetime of organic molecules represents the average duration of their excited states and the intrinsic properties of the molecule. A longer fluorescence lifetime indicates that excitons exist in the excited state for a longer period of time, which may lead to more effective charge separation (Litani-Barzilai et al., 2004; Li et al., 2024b). The excited state lifetime and fluorescence lifetime were calculated using the following equations.

$$\tau_1 = \frac{1.499}{f_{abs}{E_1}^2} \tag{7}$$

$$\tau_2 = \frac{2\pi\varepsilon_0 m_e h^2 c^3}{e^4 {E_2}^2 f_2} \tag{8}$$

where f_{abs} mean the oscillator strength of the first excited state, and E_1 means the excitation energy; e, m_e, ε_0, and h denote the *meta*-charge, the electron mass, the vacuum dielectric coefficient, and Planck's constant, respectively. E_2 and f_2 denote the emission energy and strength, and c denotes the speed of light. As shown in Table 2, the excited state lifetimes of both CS-70 and CS-72 are in the nanosecond range (3.891 ns and 4.466 ns), which facilitates the efficient electron injection process (Meti et al., 2019). In addition, the fluorescence lifetime of CS-72 (5.063 ns) was slightly larger than that of CS-70 (4.999 ns), suggesting that the molecule may have a higher fluorescence efficiency (Sun et al., 2023).

3.4. Chemical reaction parameters

To analyze the chemical reaction parameters of the molecules, ionization potential (IP), electron affinity (EA), chemical hardness (h), electrophilicity (W), and electron acceptance (W^+) were calculated as follows (Zhang and Musgrave, 2007; Delgado-Montiel et al., 2020; Singh and Kanaparthi, 2022):

$$IP = E_+ - E_0 \tag{9}$$

$$EA = E_0 - E_- \tag{10}$$

$$h = \frac{IP - EA}{2} \tag{11}$$

$$W = \frac{(IP + EA)^2}{4(IP - EA)} \tag{12}$$

Table 2
The emission wavelength (λ_{flu} in nm), oscillator strength of fluorescence state (f_2), emissive energy (E_2 in eV), stokes shift (in nm), excited state lifetime (τ_1 in ns), and fluorescent lifetime (τ_2 in ns) of CS-70 and CS-72.

Dyes	λ_{flu}	f_2	E_2	stokes shift	τ_1	τ_2
CS-70	567.71	0.967	2.184	125.87	3.891	4.999
CS-72	602.05	1.073	2.059	116.63	4.466	5.063

$$W^{+} = \frac{(IP + 3EA)^2}{16(IP - EA)} \tag{13}$$

where E_+ is the energy of the optimized cation, and E_- is the energy of the optimized anion, and E_0 is the energy of the optimized neutral molecule. In the first place, a lower IP indicates that the dye molecule more easily loses electrons and has better hole transport properties, and a higher EA indicates that the dye molecule has better electron transport properties (Zhang and Musgrave, 2007; Delgado-Montiel et al., 2020). From Table 3, we can see that compared with CS-70 (4.845eV, 2.467 eV), CS-72 has approximately equal IP (4.851 eV) and higher EA (2.813 eV), which indicates that CS-72 has better electron transport properties. The value of h (1.019 eV) of CS-72 is significantly lower than that of CS-70 (1.189 eV), which favors the transfer of charge. Subsequently, W and W^+ were used to measure the molecular stability and the ability to attract electrons from the external environment, and dye with higher W indicates better energetic stability of the molecule and higher W^+ denotes better electron-absorbing ability (Singh and Kanaparthi, 2022). The W (7.205 eV) and W^+ (5.416 eV) of CS-72 were higher than those of CS-70 (5.619 eV, 3.939 eV), which suggests that CS-72 has better stability and a stronger ability to acquire electrons from outside.

3.5. Nonlinear optical properties

Nonlinear optical properties study the nonlinear relationship between the response of a substance under the action of intense light and the field strength (Huang et al., 2021). Polarizability (α) and first hyperpolarizability (β) are essential parameters for probing the nonlinear optical properties of molecules in electronics. The polarizability is calculated as follows (Senge et al., 2007):

$$\alpha = \frac{\alpha_{xx} + \alpha_{yy} + \alpha_{zz}}{3} \tag{14}$$

Where α_{xx}, α_{yy}, and α_{zz} denote the tensor components of polarizability, respectively. The β tensor represents the result of the third-order derivative of the energy (Patil et al., 2018):

$$\beta_{tot} = \sqrt{\beta_x^{\,2} + \beta_y^{\,2} + \beta_z^{\,2}} \tag{15}$$

Where the x-component β_x is obtained from relationship $\beta_x = \beta_{xxx} + \frac{1}{3}\sum_{j\neq x}\left(\beta_{xjj} + \beta_{jxj} + \beta_{jjx}\right)$. The β_{xxx}, β_{xxy}, β_{xyy}, β_{yyy}, β_{xxz}, β_{xyz}, β_{yyz}, β_{xzz}, β_{yzz}, and β_{zzz} denote the tensor components in each direction of the first hyperpolarizability, respectively. The better NLO properties indicate that the molecule has a more sensitive response to electromagnetic fields, which can lead to better charge transfer properties of the molecule. Molecules with high nonlinear optical properties are more likely to produce charge transfer excitations and a strong degree of electron delocalization. The α and β data for the monomeric molecules are presented in Table S2. The more pronounced polarizability polarization tensors for the CS-70 molecules are XX, YY, and ZZ, which are 1021.16 a.u., 593.62 a.u., and 281.21 a.u., respectively. When the auxiliary receptor was changed to naphthobisthiadiazole, the three tensors were increased to 1291.32 a.u.,646.19 a.u., and 430.64 a.u. The increase in the XX tensor indicates a significant increase in the molecular dipole moment in the X-direction (from triphenylamine to carboxyl group), meaning that the charge transfer of CS-72 will be more significant under the action of the electric field. The first hyperpolarizability can be used to describe the trend of molecular polarizability in an electric field. The maximum components of both molecules are XXX tensor (85434.20 a.u. of CS-70 and 148333.00 a.u. of CS-72). The larger XXX component of CS-72 suggests that its polarizability increases more dramatically with electric field strength. The total first hyperpolarizabilities of CS-70 and CS-72 are 85086.29a.u. and 148237.77a.u., respectively. And total first hyperpolarizabilities indicating that the change in the polarizability is positively correlated with the change in the electric field strength. The larger total first hyperpolarizability of CS-72 may be attributed to the enhancement in the dipole moment of the molecule, which produced good optical response and charge transfer characteristics.

Table 3
Ionization potential (IP in eV), Electron affinity (EA in eV), Chemical hardness (h in eV), electrophilicity (W in eV), and electro-accepting power (W^+ in eV).

Dyes	IP	EA	h	W	W^+
CS-70	4.845	2.467	1.189	5.619	3.939
CS-72	4.851	2.813	1.019	7.205	5.416

3.6. Intramolecular charge transfer

To further analyze the ICT phenomenon, we performed a hole-electron analysis of the first excited state of the dye molecule. The calculated charge transfer distance (D_{CT}), average charge distribution span (H), charge overlap (Sr), and coulomb attraction energy (E_c). Here, D_{CT} is defined as the distance between the center of mass of the electron and the hole, and H reflects the overall average breadth of the distribution of electrons and holes, with a larger H indicating a wider distribution. Sr is used as a measure of the degree of overlap of the charges, with a larger Sr indicating a higher degree of overlap (Liu et al., 2020). In addition, a smaller Ec is favorable for the current generation because exciton dissociation requires overcoming Ec to separate electrons from holes. The relevant parameters are listed in Table 4, and Fig. S3 shows a hole-electron isosurface diagram to visualize the distribution of holes and electrons, where purple color stands for hole density and blue color stands for electron density, respectively. According to the data presented in Table 4, it is evident that CS-72 exhibits larger values for D_{CT} (4.153 Å) and H (4.283 Å) compared to CS-70 (3.915 Å, 3.773 Å), meaning that CS-72 possesses a greater charge transfer distance and a wider extension of electron-hole distribution. Additionally, the Sr value of CS-72 (0.557 Å) is smaller than that of CS-70 (0.573 Å), meaning a reduced overlap between the holes and electrons in CS-72. These findings collectively suggest that CS-72 may possess superior ICT properties to promote photoelectric and NLO performance, which can be attributed to the enhanced electron-withdrawing ability of the naphthobisthiadiazole moiety. In addition, compared with CS-70 (3.339 eV), the CS-72 has a smaller E_C (2.830 eV), so it is easier to be excited and subsequently injected into the CB, which indicates that CS-72 may produce a larger photocurrent.

3.7. CDD and electron injection processes

The CDD map serves as a powerful tool to visually represent the charge transfer occurring within dye@TiO_2 complexes, providing insights into the distribution of electrons and holes (Zhang et al., 2012). In Fig. 5, we have meticulously plotted the CDD maps for the excited states S1-S6 of the dye@TiO_2 complexes. In the S1 excited state, the hole density predominantly resides in the donor triphenylamine, with a lesser extent in the auxiliary acceptor. As for the electron density, it primarily localizes in the auxiliary acceptor, with a few electrons beginning to emerge in TiO_2. This observation signifies the initiation of the electron injection process. For CS-70, the S2-S5 states exhibit a similar distribution pattern for both electrons and holes, and the holes are predominantly distributed in both the donor and the auxiliary acceptor, while

Table 4
Parameters of charge-separated distance (D_{CT} in Å), the mean charge distribution span (H in Å), the overlap degree of charge (Sr in Å), and coulomb attraction energy (E_c in eV) of all dyes.

Dyes	D_{CT}	H	Sr	E_c
CS-70	3.915	3.773	0.573	3.339
CS-72	4.153	4.283	0.557	2.830

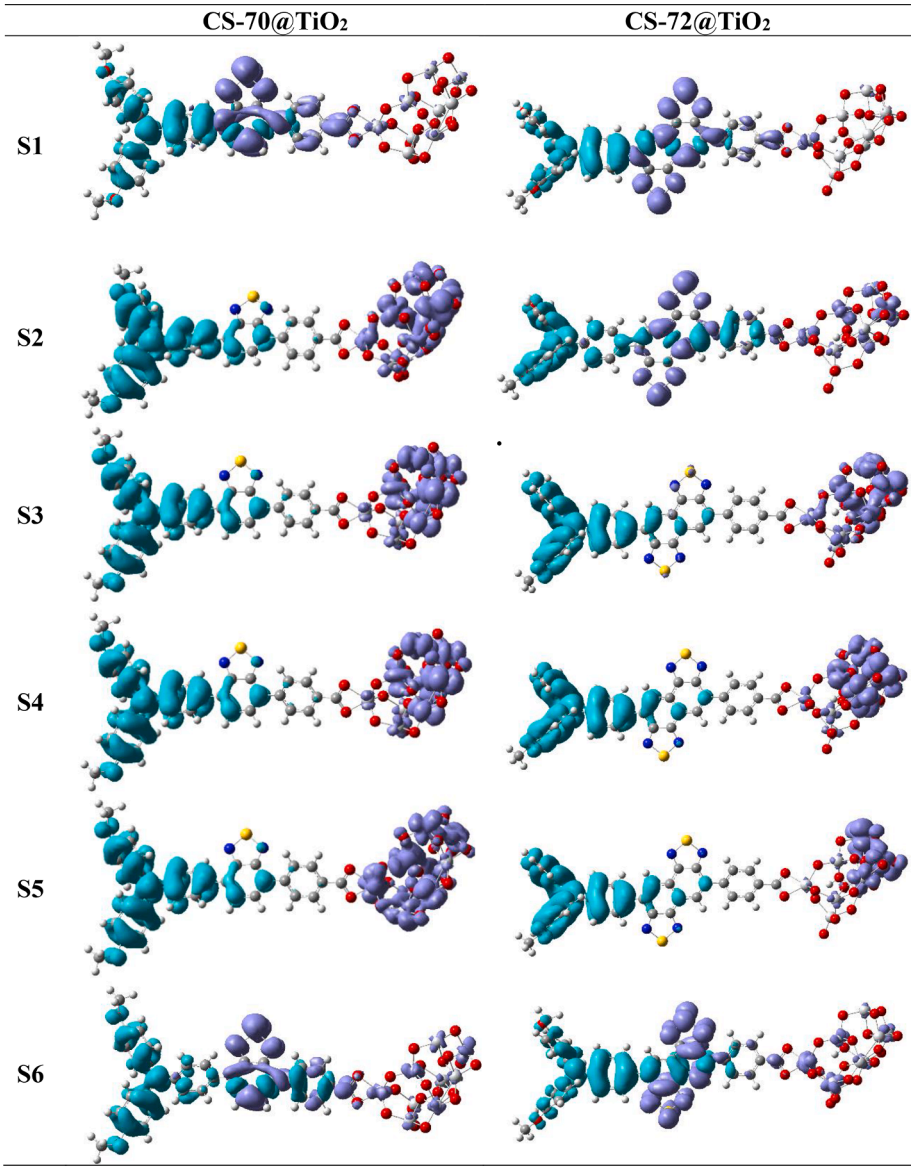

Fig. 5. The charge density difference (CDD) (the electron density areas covered with purple and hole density areas covered with cyan) of the excited state S1–S6 for dyes that are bound to the TiO_2 surface.

the electrons are effectively injected into the titanium dioxide. Notably, a pronounced charge separation between holes and electrons is evident, facilitating efficient electron injection. In the case of CS-72, within the S2 excited state, holes are still primarily localized in the donor, while electrons appear in the secondary acceptor and titanium dioxide. Substantial charge separation is observed in the S3-S5 states. It is worth mentioning that the above figure reveals a discrepancy in the number of electrons injected into TiO_2 by CS-72 compared to CS-70.

To elucidate the underlying cause for this discrepancy, we conducted calculations of the adsorption energies (E_{ads}) and chemical bonding parameters between the dye and the semiconductor. These parameters are vital in determining the interaction strength between the dye and the semiconductor, as well as serving as indicators of electron transmittance (Dolatabadi et al.,2021; Yang et al., 2023). The E_{ads} can be derived through the following equation:$E_{ads} = E_{dye/TiO_2} - \left(E_{dye} + E_{TiO_2}\right)$, where E_{dye/TiO_2} is the total energy of the dye@TiO_2 complex, and E_{dye} is the energy of the single dye molecule in the complex and E_{TiO2} is the energy of TiO_2 in the complex. Additionally, the chemical bonding parameter is characterized by the bond length of the Ti-O bond. Table S3 Shows the bond lengths between all the Ti-O atoms fall within the range of 2.059–2.070 Å. Notably, E_{ads} values for CS-70 and CS-72 are −86.42 kcal/mol and −80.01 kcal/mol, respectively, indicating successful adsorption of both molecules onto the TiO_2 film (Ullah, 2017; Dolatabadi et al., 2022a), and CS-70 displays a more substantial negative binding energy, indicating a stronger affinity for binding to the semiconductor and promote electron injection. The relatively weaker binding capability of CS-72 could be linked to its larger molecular size, leading to less compact aggregation on the TiO_2 surface.

The ground state redox potential (E_{OX}), excited state redox potential

Table 5
The electron injection driving force (ΔG^{inject} in eV), the oxidation potential dye in the ground state(E_{OX} in eV), the oxidation potential dye in an excited state (E^*_{OX} in eV), and the dye regeneration driving force (ΔG_{reg} in eV).

Dyes	E_{OX}	E^*_{OX}	ΔG^{inject}	ΔG_{reg}
CS-70	4.821	2.015	−1.985	0.221
CS-72	4.855	2.301	−1.699	0.255
CS-70-Chl	4.885	2.817	−1.183	0.284
CS-72-Chl	4.989	2.998	−1.002	0.389

(E^*_{OX}), electron injection driving force (ΔG^{inject}), and electron regeneration driving force (ΔG_{reg}) were calculated and are displayed in Table 5, and the calculation equations are as follows (Li et al., 2014, Britel et al., 2022):

$$\Delta G^{inject} = E^*_{OX} - E_{CB} \quad (16)$$

E_{CB} denotes the energy level of band of conduction, usually using 4.0 eV.

$$\Delta G_{reg} = E\left(I_3^-/I^-\right) + E_{OX} \quad (17)$$

where $E(I_3^-/I^-)$ represents the energy of the iodide ion in the electrolyte solution, usually using −4.6 eV. Both molecules' negative ΔG^{inject} (−1.985 eV, −1.699 eV) signifies their efficient electron injection into the semiconductor titanium dioxide (Balraju et al., 2009; Saji and Pyo, 2010). Regarding ΔG_{reg}, CS-72 (0.255 eV) exhibits a higher regeneration ability than CS-70 (0.221 eV). Fig. S4 displays molecular ESP maps to delve deeper into their REDOX reaction sites occur, which serves to analyze intermolecular interactions and predict reaction sites and positions (Murray and Politzer, 2011). The color gradient from blue to white to red represents a gradual increase in electrostatic potential. A higher ESP value for two dyes indicates a greater affinity for nucleophilic reagents, facilitating the binding with negatively charged iodide ions in the electrolyte solution for dye regeneration. The positive portion of ESP for CS-70 and CS-72 is mainly distributed on triphenylamine derivatives, suggesting that atoms in the donor region are more susceptible to iodide bombardment for dye regeneration. In addition, the maximum ESP values of the CS-72 are generally higher than those in the CS-70, which also indicates that the CS-72 has a stronger regenerative capacity.

3.8. Dye aggregation

Dye molecules aggregation detrimentally impacts the photovoltaic characteristics of the solar cell because of intermolecular interactions (Wuerthner et al., 2011). Specifically, H-type aggregation arises from intermolecular hydrogen bonding and week interaction between two monomers, typically categorized as head-to-head (H-H) and head-to-tail (H-T). So, we investigated the potential for dimer formation of the examined face-to-face dyes (Dell'Orto et al., 2012; Nachimuthu et al., 2016). The structure of the optimized dimer is illustrated in Fig. 6, and the intermolecular interaction energy (ΔE) and average intermolecular distance (D) were calculated and presented in Table 6. For calculating ΔE, the CS-70: H-H (−1.45 eV) < H-T (−1.36 eV), and CS-72: H-H (−1.92 eV) < H-T (−1.87 eV), indicating that the H-H type structure is more stable and a greater possibility in the head-to-head aggregating manner for the two molecules. According to D, for H-H: CS-72 (3.58 Å) > CS-70 (3.40 Å), and for H-T: CS-72 (3.38 Å) > CS-70 (3.12 Å). CS-72 molecules, with larger average intermolecular distances, will exhibit a reduced propensity for dye aggregation, which can be attributed to the fact that CS-72 possesses a more distorted structure that hinders the occurrence of dye aggregation. In the case of CS-70, its propensity for increased aggregation may negatively impact the performance of DSSCs in practical applications. The excessive accumulation of dyes on the TiO_2 surface can result in several detrimental effects. Firstly, it triggers excited state quenching, diminishing charge separation and light absorption efficiency. Secondly, dye accumulation hinders charge transport pathways, reducing injected electrons and lowering the *Voc*. For the above cases, incorporating specific anti-aggregation agents such as chenodeoxycholic acid (CDCA) or deoxycholic acid (DCA) has been demonstrated as a beneficial strategy in numerous studies, and is also extensively applied in the production of DSSCs.

Table 6
Simulated intermolecular average distance (D in Å), and interaction energies (ΔE in eV) of the dimers in H-H and H-T types for the isolated monomers.

Dye	CS-70		CS-72	
	H-H	H-T	H-H	H-T
D	3.40	3.12	3.58	3.38
ΔE	−1.45	−1.36	−1.92	−1.87

3.9. J_{SC}, Voc and efficiency prediction

The *PCE* serves as an absolute indicator for evaluating the performance of dye-sensitized solar cells. As seen in Equation (1), enhancing *Jsc* and *Voc* is crucial for improving cell performance. From *Voc* calculation, the difference between the quasi-Fermi energy levels of the sensitized semiconductor and the redox pair (ΔE_{CB}), as well as the amount transferred to the semiconductor TiO_2 (n_c), directly impact the magnitude of *Voc* (Huaulme et al., 2020; Sultan et al., 2020). The calculated PDOS of the dye-titanium dioxide is presented in Fig. 7, and the ΔE_{CB} was determined using a linear fitting method. The ΔE_{CB} of CS-72 (0.0307 eV) is more pronounced compared to that of CS-70 (0.0289 eV), theoretically resulting in a larger *Voc*. However, Table 7 shows that the *Voc* of CS-70 (0.633 V) is slightly greater than that of CS-72 (0.623 V), indicating that n_c has a more significant influence on *Voc*. As indicated in Table 7, the n_c of CS-70 (0.3501×10^{18} cm^{-3}) is significantly higher than that of CS-72 (0.2310×10^{18} cm^{-3}). Considering both ΔE_{CB} and n_c provides a reasonable explanation for the similar *Voc* values of the two dyes. The theoretically calculated data align well with the

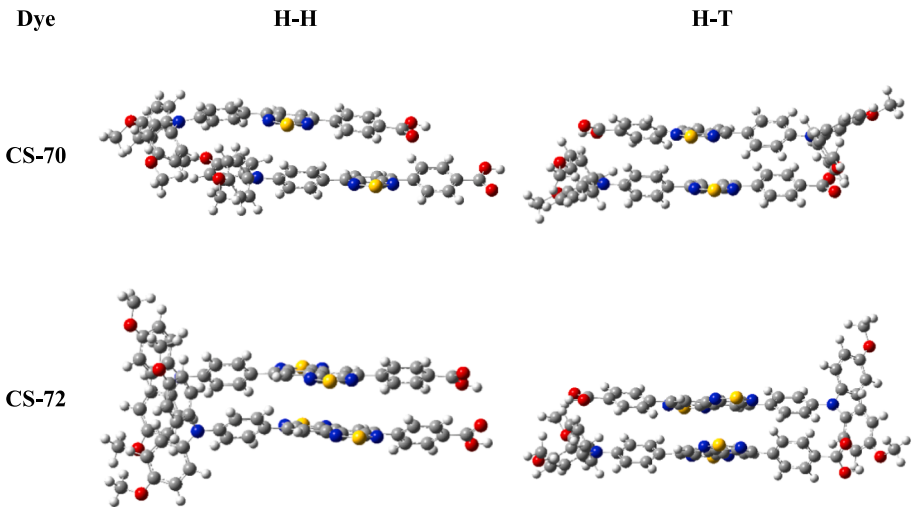

Fig. 6. The optimized dimer geometries in Face-Face (H-H and H-T).

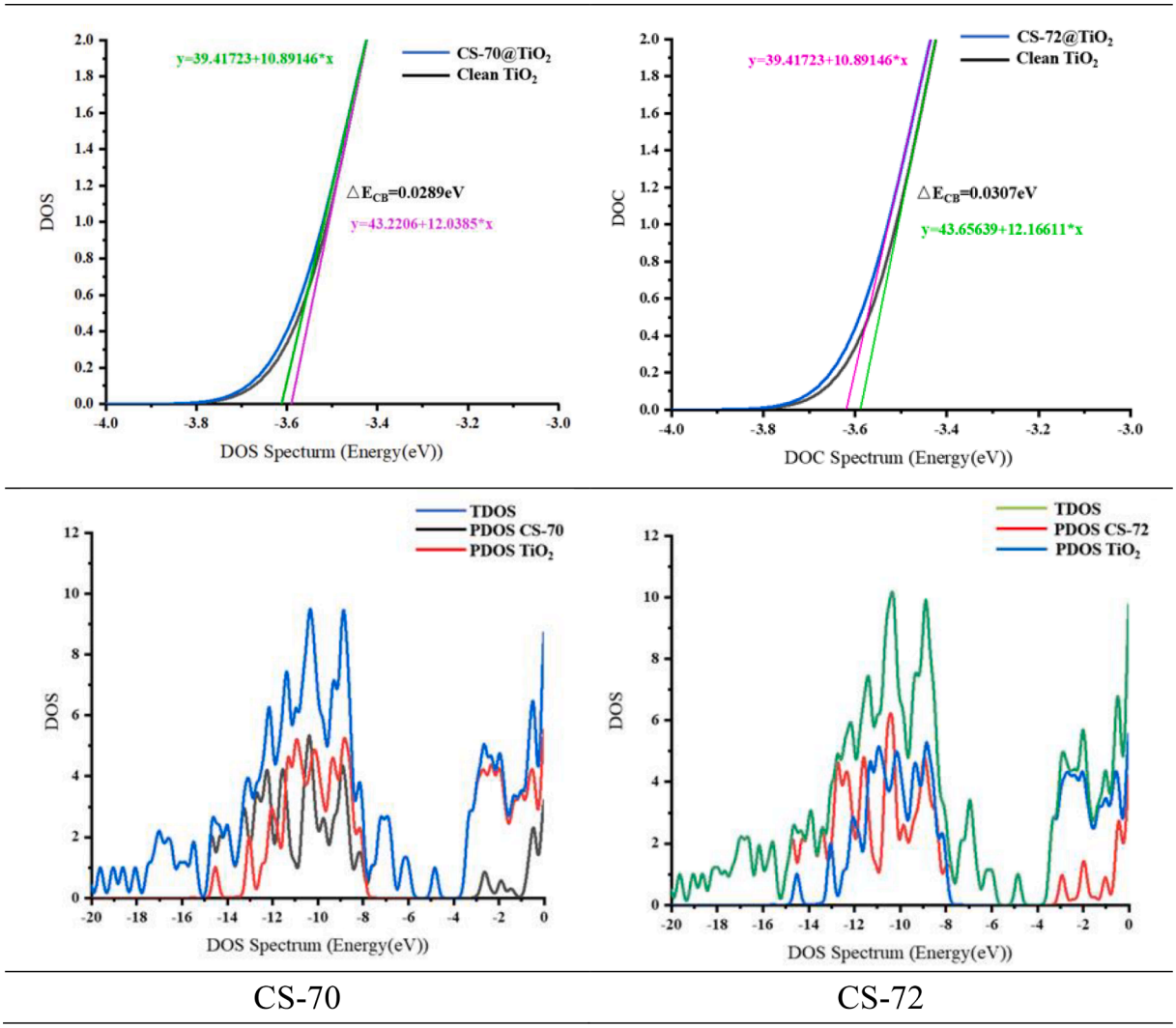

Fig. 7. Calculation of the conduction band shift (ΔE_{CB}) and partial density of states (PDOS).

Table 7
The estimated redox potential (E_{redox} in eV), numbers of electrons (n_c in cm^{-3}), the conduction band shift (ΔE_{CB} in eV), and obtained photovoltage (Voc in V) of all investigated dyes.

Dyes	E_{redox}	$n_c \times 10^{18}$	ΔE_1*	ΔE_{CB}	V_{OC}
CS-70	−4.80	0.3501	−0.1370	0.0289	0.633
CS-72	−4.80	0.2310	−0.2072	0.0307	0.623

*$\Delta E_1 = K_B T \ln(n_c/N_{CB})$.

experimental results.

Regarding *Jsc*, a higher light trapping capacity leads to increased photocurrent (Ma et al., 2014; Chen et al., 2022). The LHE plots of CS-70 and CS-72 are illustrated in Fig. 8, and the light absorption range of CS-70 primarily falls within 300–600 nm, while that of CS-72 extends to 300–700 nm. The replacement of benzothiadiazole with naphthobisthiadiazole significantly widens the light-trapping region and enhances light-trapping ability. Consequently, a larger photocurrent is generated, favorably contributing to increased *PCE*. The calculated *Jsc* values are presented in Table 8, where CS-72 (19.29 mA/cm^2) surpasses CS-70 (14.84 mA/cm^2), consistent with the experimental sequence. According to Eq. (1) and the following equations, the *PCE* values of the two molecules were calculated, and the data are shown in Table 8, and the solar cell I-V curves were simulated as shown in Fig. 9. The calculation formula is as follows (Duvva et al., 2020; Zhao et al., 2021):

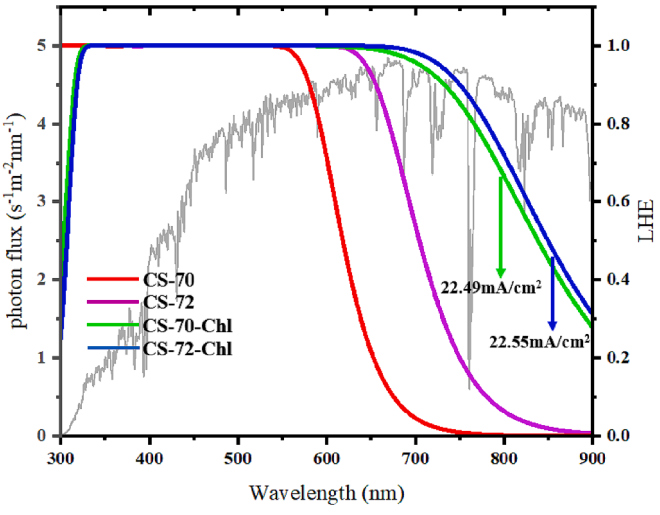

Fig. 8. The simulated light-harvesting efficiency LHE (λ) of isolated and co-sensitized dyes, and the gray line is the Air Mass 1.5 Global (AM 1.5G) solar spectrum irradiation.

Table 8
The estimated open-circuit voltage (*Voc* in V), short-circuit photocurrent density (*Jsc* in mA/cm^2), fill factor(*FF*), and photoelectric conversion efficiency (*PCE* in %).

Dyes	Predict data				Experimental data		
	Jsc	*Voc*	*FF*	*PCE*	*Jsc*	*Voc*	*PCE*
CS-70	14.84	0.633	0.834	7.83	13.49	0.734	6.59
CS-72	19.29	0.623	0.832	10.00	14.31	0.730	7.17

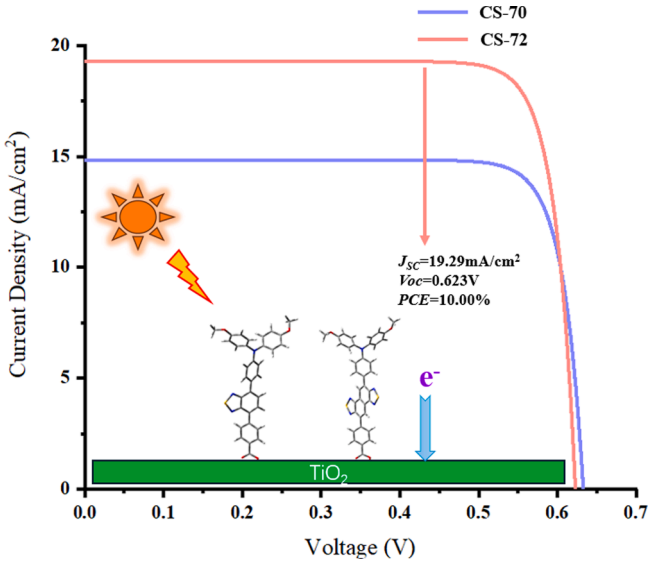

Fig. 9. The simulated photocurrent-potential (I-V) characteristics of CS-70 and CS-72.

$$V = \frac{K_B T}{e} ln\left(\frac{J_{SC} - I}{I_S} + 1\right) \tag{18}$$

$$I_S = \frac{J_{SC}}{exp\left(\frac{eV_{OC}}{K_B T}\right) - 1} \tag{19}$$

$$FF = \frac{I_m V_m}{J_{SC} V_{OC}} \tag{20}$$

K_B is the Boltzmann constant, and T is the temperature (300 K), and I_S denotes reverse saturation current, and $I_m V_m$ means maximum power (This is the maximum value of the product of I and V), and *FF* is the fill factor. As shown in Table 8, since CS-72 has a significantly higher J_{SC} than CS-70, and has a similar *Voc* as CS-70, this results in a significantly higher *PCE* (10.00 %) than (7.83 %) for CS-72, which is in agreement with the experimental trend (Cui et al., 2023).

3.10. Structure and excited state properties of co-sensitized system

In terms of molecular design, Chlorophyll derivatives H_2Chl was used as the sensitizer to co-sensitize the monomer small molecules, and the co-sensitization systems were named CS-70-Chl and CS-72-Chl, separately. To investigate the stability of the co-sensitized molecules, energy decomposition analysis based on forcefield (EDA-FF) was performed on the co-sensitized molecules, and the total interaction energy was also calculated (Li et al., 2021; Lu and Chen, 2023). The energy of the total interaction energy can be calculated from the following equation: $\Delta E = E_{dimer} - \sum_i E_i^{fragment}$. Moreover, the total interaction energy is decomposed in the following form: $\Delta E = \Delta E_{orb} + \Delta E_{disp} + \Delta E_{els} + \Delta E_{xrep}$, where ΔE_{orb} (orbital interaction energy) is the energy change due to mixing between occupied and unoccupied orbitals from inside and between fragments, and ΔE_{disp} (dispersive interaction energy) comes from dispersive weakly attractive interactions, and ΔE_{els} (electrostatic interaction energy) comes from classical electrostatic interactions between the fragments, and the ΔE_{xrep} (exchange-mutual repulsion interaction energy) embodies the contribution of exchange–correlation effects to the interaction energy of the fragments as well as the energy elevation between the electrons of the different fragments to satisfy the Pauli mutual repulsion principle. The nature of the interactions between the dimer fragments can be clearly understood from the data in Table 9, i.e., the interactions of both molecules are dispersion-dominated, −61.19 kcal/mol for CS-70-Chl and −73.38 kcal/mol for CS-72-Chl, respectively; orbital interactions account for a smaller portion of the interactions, −18.54 kcal/ mol and −21.47 kcal/mol for two dyes; the electrostatic interactions of the two co-sensitized molecules are −1.03 kcal/mol and −3.75 kcal/mol, respectively, which are almost negligible; the exchange-mutual repulsion energies of the two molecules are 38.38 kcal/mol and 48.83 kcal/mol, respectively, which also occupy a larger part and largely counteract the attractive effect of dispersion. In summary, the order of the interaction energies of the two co-sensitized molecules is CS-72-Chl (−49.77 kcal/mol) < CS-70-Chl (−42.38 kcal/mol), which suggests that the dimer composed of CS-72 and H_2Chl is a more stable configuration. To further examine the chemical bonding and weak interactions of the co-sensitized molecules, the heterodimer molecules were graphically represented using the interaction region indicator (IRI) method (Lu and Chen, 2021) and displayed in Fig. 10. In Fig. 10(a), the horizontal coordinate represents the sign of the second largest eigenvalue of the Hessian matrix of electron density (ρ(r)) multiplied by electron density (λ_2), which is the sign (λ_2)ρ, and the vertical coordinate is the IRI gradient function. In addition, a structural image of the heterodimer was produced in Fig. 10(b) to visualize the covalent bonds and weak interactions, and the specific meaning of each color scale is also presented. As can be seen from Fig. 10 (a), there are obvious spikes in the low gradient part (IRI < 0.5a.u.) and sign(λ_2)ρ < -0.02a.u. with blue color, which demonstrates that the two co-sensitized molecules have a stabilizing interaction with attractive hydrogen bonds. Meanwhile, a lot of spikes appear in the forward part of the sign(λ_2)ρ ≥ 0.02 in the low gradient part (IRI < 0.5a.u.) of the two heterodimers, which confirms the de-stereospecificity of the two heterodimers. In addition, for the low gradient part (IRI < 0.5 a.u.), there is also a clear sharp peak in this area of −0.02 a.u. < sign(λ_2)ρ < 0.01 a.u., which indicates that there is a stable dispersive attraction in the co-sensitized molecules. This is also evident in Fig. 10(b) that the isosurface map is essentially green between the two monomer molecules, which indicates that van der Waals forces are the dominant form of weak interaction. Strong intra-ring site-barrier interactions and weak hydrogen-bonding attraction are also represented and mainly present within the two monomer molecules themselves.

Fig. 2 shows the HOMO, LUMO, and energy gap of the single dye molecule H_2Chl and the two co-sensitized systems. The HOMO and LUMO of H_2Chl are calculated to be −5.21 eV and −2.69 eV, respectively. In the context of a co-sensitized system, the overall HOMO tends to decrease compared to CS-70 and CS-72 (measured at −4.88 eV for CS-70-Chl and −4.98 eV for CS-72-Chl). The LUMO of CS-70-Chl also decreases significantly to −2.67 eV, while there is no significant change in the LUMO of CS-72-Chl. Both co-sensitized systems still exhibit effective electron injection and regeneration properties. The excited state properties of H_2Chl are detailed in Table 1, where it is noted that chlorophyll

Table 9
The calculated orbital interaction (ΔE_{orb}), dispersion energy (ΔE_{disp}), electrostatic interaction (ΔE_{els}),exchange-repulsion interaction (ΔE_{xrep}), as well as total interaction energy (ΔE) of heterodimers (unit: kcal/mol).

Dyes	ΔE_{orb}	ΔE_{disp}	ΔE_{els}	ΔE_{xrep}	ΔE
CS-70-Chl	−18.54	−61.19	−1.03	38.38	−42.38
CS-72-Chl	−21.47	−73.38	−3.75	48.83	−49.77

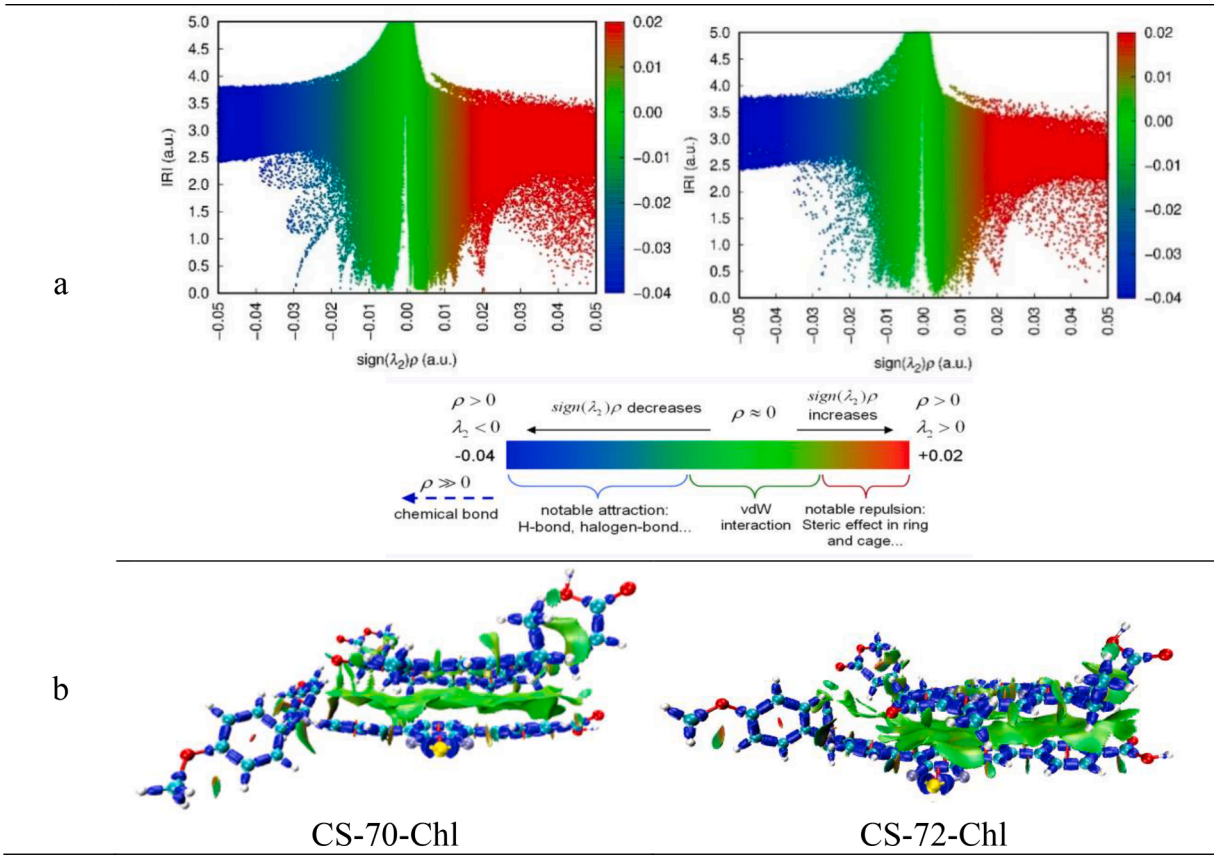

Fig. 10. (a) IRI vs sign(λ_2)ρ scatterplot of co-sensitized molecules, and detailed description of the color scale of the IRI vs sign(λ_2)ρ scatterplot. (b) Isosurface plots of the weak interactions of the co-sensitized fractions using the IRI method.

based on the chlorin π-system typically shows two characteristic absorption bands: the Soret band and the Q_y band. The calculated Soret band and Q_y band for H_2Chl are in the ranges of 350–450 nm and 550–700 nm, respectively, and its main absorption peaks are identified as the S3 state (394.80 nm) and the S1 state (605.17 nm), corresponding to the Soret band and Q_y band, respectively. Comparatively, H_2Chl maintains good absorption in the 600–800 nm range, making it a suitable co-adsorbent to enhance solar spectrum utilization and increase the *PCE*. Excitation properties of the S1-S10 states for the co-sensitized molecules were also calculated (the S1-S6 in Table 1 and S7-S10 in Table S4), revealing broader spectra for the dimer molecules. The maximum absorption wavelengths for CS-70-Chl and CS-72-Chl are 612.81 nm and 622.84 nm, respectively, with transition modes of H-1 → L (0.63) and H → L+1 (0.45) and oscillator intensities of 0.188 and 0.151, respectively. Notably, a new characteristic peak is observed for the S7 states of CS-70-Chl and CS-72-Chl at 400.69 nm (f = 1.337) and 405.60 nm (f = 1.372), involving transitions of H-1 → L+2 (0.52) and H → L+2 (0.52), respectively. From the absorption spectra in Fig. 4, it is also evident that the spectral range of the co-sensitized molecules is broadened, and the molar extinction coefficient is significantly enhanced, which is conducive to the generation of larger photocurrents.

3.11. *Intermolecular charge transfer and enhanced photoelectric properties*

The estimation of intermolecular charge transfer involves the calculation of electron and hole contributions from dye fragments, as well as the intermolecular electron transfer in each heterodimer (Wang et al., 2021; Yang et al., 2022; Li et al., 2023). Fig. 11 illustrates the charge transfer in the S1-S10 states of the co-sensitized molecules using CDD. It is observed that for CS-70-Chl, there are only H_2Chl participation in the excitation of the S1, S2, and S8 states, and only CS-70 participates in the excitation in the S3 state; for CS-72-Chl, the H_2Chl exclusively contributes to the S1 and S7 states, and the above excited states are localized on a certain molecule. Furthermore, ICT process can be found forS4, S6, and S7 states of CS-70-Chl, which shows obvious electron transfer from H_2Chl to CS-70; while for CS-72-Chl, it shows obvious electron transfer from H_2Chl to CS-72 in the S2, S4, S5, S9 and S10 states. The number of transferred electrons was calculated and presented in Table 10, while the percentage of hole-electron distribution was listed in Table S5. Taking the S4 state of CS-70-Chl as an example, the majority of holes are located on H_2Chl (98.54 %), while electrons are primarily on benzothiadiazole (75.59 %), resulting in a charge transfer of 0.9420e. Similarly, in the S6 and S7 states of CS-70-Chl, H_2Chl holds most of the holes (98.41 %, 97.64 %), and the auxiliary acceptor contains the electrons (69.65 % and 87.55 %), with transferred charges of 0.8692e and 0.1009e, respectively. In CS-72-Chl, the S2 state of H_2Chl carries the majority of holes (78.48 %), with naphthobisthiadiazole holding the electrons (66.21 %), resulting in a charge transfer of 0.5449e. The transferred charges in the S4, S5, S9 states are 0.3494e, 0.9029e, and 0.2428e, respectively. In the S10 state, holes are mainly on H_2Chl (59.44 %), while electrons are predominantly on naphthobisthiadiazole (83.88 %), with a charge transfer of 0.5370e. Overall, CS-72-Chl demonstrates a higher number of charge transfer excited states, indicating superior charge transfer properties.

To analyze the electron injection and regeneration of the co-sensitized models, their electron injection driving energies and redox potentials were calculated in Table 5. The ΔG^{inject} of both CS-70-Chl and CS-72-Chl were negative (−1.183 eV, −1.002 eV), which theoretically confirms the feasibility of the electron injection of the co-sensitized molecules. The ΔG_{reg} were calculated to be 0.284 eV and 0.389 eV, respectively, indicating that the regeneration ability of the co-sensitized

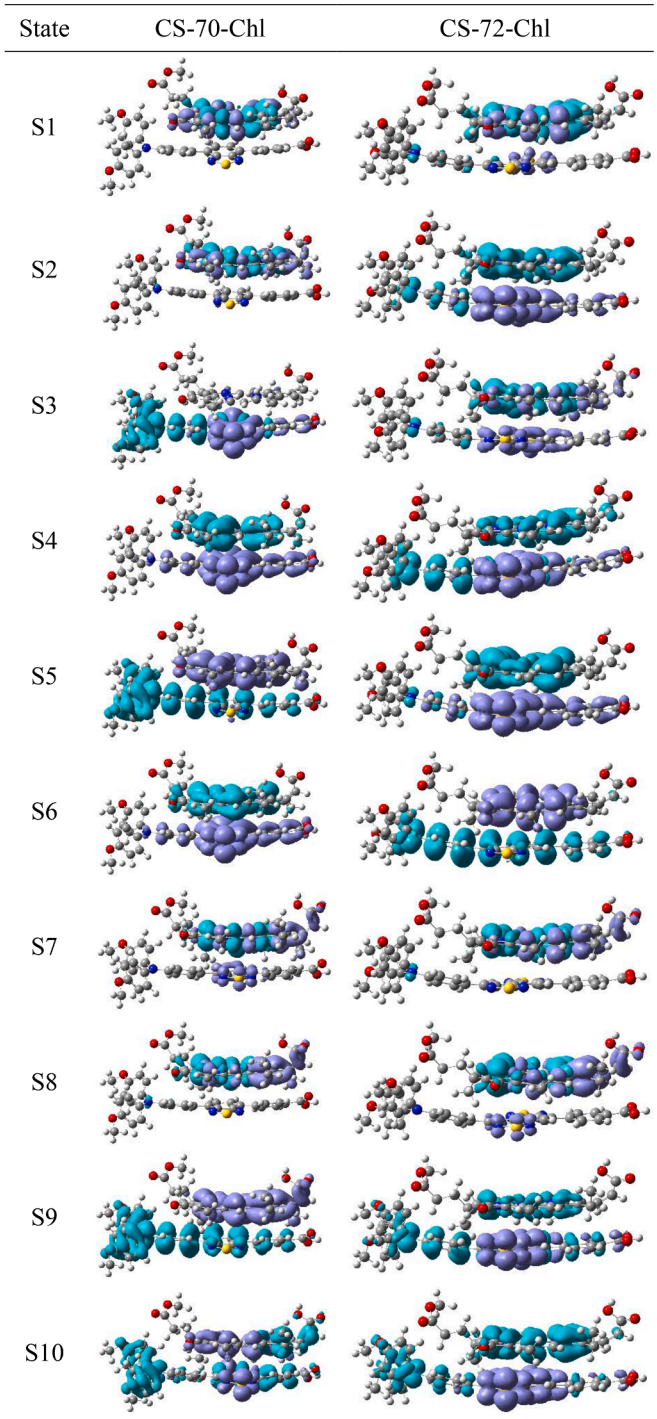

Fig. 11. The charge density difference (CDD) of electron transition in co-sensitized films.

model was significantly improved compared to the monomeric dye molecules, which should be attributed to the introduction of H_2Chl to increase the overall ground-state oxidation potential, which was more favorable for the reaction with the electrolyte solution. The enhanced regeneration capacity facilitates the sustained and efficient operation of the DSSC. In order to further measure the effect of the introduction of H_2Chl on the photocurrent, LHE plots were made based on the absorption spectra and the J_{SC} of the co-sensitized models were calculated. As can be seen in Fig. 8, the two co-sensitized models showed a significant enhancement of the light trapping ability, which is conducive to the full absorption of sunlight and the realization of the panchromatic

Table 10
The amount of intermolecular charge transfer between the various fragments of the co-sensitized film (e).

Dye	state	H_2Chl-D	H_2Chl −A′	H_2Chl −π	H_2Chl −A	H_2Chl −Dye
CS-70-Chl	S4	0.0752	0.7448	0.0991	0.0229	0.9420
	S6	0.0715	0.6846	0.0914	0.0217	0.8692
	S7	0.0004	0.0824	0.0148	0.0033	0.1009
CS-72-Chl	S2	0.0010	0.5017	0.0348	0.0074	0.5449
	S4	0.0062	0.3134	0.0245	0.0053	0.3494
	S5	0.0488	0.7756	0.0652	0.0133	0.9029
	S9	−0.0166	0.2365	0.0165	0.0064	0.2428
	S10	0.0035	0.4913	0.0323	0.0098	0.5370

sensitization, and the CS-72-Chl demonstrated the largest J_{SC} (22.55 mA/cm^2), which is expected to be a strong candidate for the sensitization of H_2Chl.

4. Conclusion

This study delves into the microscopic mechanisms at a theoretical level, focusing on the CS series dyes photoelectric performance of and the co-sensitization with chlorophyll derivatives on solar cell performance. The investigation begins with exploring the effects of benzothiadiazole and naphthobisthiadiazole as auxiliary receptors on the photovoltaic performance of the molecules. The results reveal that naphthobisthiadiazole, due to its more extended conjugated structure, significantly reduces the orbital energy gap by 0.33 eV and red-shifts the maximum absorption peak of the molecule by 43.58 nm compared to benzothiadiazole. Moreover, naphthobisthiadiazole exhibits stronger electron absorption, with a higher orbital contribution in LUMO. Its introduction enhances the molecule's D_{CT}, H, α, and β_{tot} while lowering Sr and E_C, thereby improving the molecule's ICT properties. Additionally, introducing naphthobisthiadiazole reduces aggregation probability, promotes interaction with the electrolyte solution, and supports stable DSSC operation. The amalgamation of these factors results in CS-72 exhibiting superior *Jsc* (19.29 mA/cm^2) and *PCE* (10.00 %).

Subsequently, the study incorporates H_2Chl as a co-sensitizer, deeply investigating the intermolecular interactions, orbital energy levels, spectra characters, and charge transfer properties of the co-sensitized system. The findings reveal a noticeable dispersive attraction between the molecules, contributing to the overall stability of the system. The orbital energy levels of the co-sensitized system align well with the requirements for electron injection and dye regeneration processes. Moreover, the incorporation of H_2Chl results in a significant widening of the light trapping region, expanding it from 600 nm to 800 nm. This extension is instrumental in achieving panchromatic absorption, enhancing the overall light absorption capabilities of the system. Overall, the study demonstrates the feasibility of enhancing the *PCE* of J_{SC} through chlorophyll and its derivatives co-sensitization. The J_{SC} of CS-72 after co-sensitization with H_2Chl reaching 22.55 mA/cm^2 as a promising dye candidate for improved solar cell performance.

CRediT authorship contribution statement

Baishuo Li: Data curation, Formal analysis, Investigation, Writing – original draft, Writing – review & editing. **Jiayu Han:** Data curation, Writing – review & editing. **Peng Song:** Project administration. **Yuanzuo Li:** Project administration, Resources, Software.

Declaration of Competing Interest

The authors declare that they have no known competing financial interests or personal relationships that could have appeared to influence

the work reported in this paper.

Acknowledgments

This work was supported by National Natural Science Foundation of China (Grant No. 12074059 and 11404055) and the College Student Research Training Program of Northeast Forestry University (DC-2024115).

Appendix A. Supplementary data

Supplementary data to this article can be found online at https://doi.org/10.1016/j.arabjc.2024.105799.

References

Adamo, C., Jacquemin, D., 2013. The calculations of excited-state properties with Time-Dependent Density Functional Theory. Chem. Soc. Rev. 42 (3), 845–856. https://doi.org/10.1039/c2cs35394f.

Alizadeh, A., Roudgar-Amoli, M., Bonyad-Shekalgourabi, S.-M., Shariatinia, Z., Mahmoudi, M., Saadat., F., 2022. Dye sensitized solar cells go beyond using perovskite and spinel inorganic materials: A review, *Renew. Sust. Energ. Rev.* **157**, 112047; 10.1016/j.rser.2021.112047.

An, J., Tian, Z., Zhang, L., Yang, X., Cai, B., Yu, Z., Zhang, L., Hagfeldt, A., Sun, L., 2021. Supramolecular Co-adsorption on TiO_2 to enhance the efficiency of dye-sensitized solar cells. J. Mater. Chem. A 9, 13697–13703. https://doi.org/10.1039/D1TA00807B.

Arslan, B. S., Güzel, E., Kaya, T., Durmaz, V., Keskin, M., Avcı, D., Nebioğlu, M., Şişman, İ., 2019. Novel D-π-A organic dyes for DSSCs based on dibenzo[b,h][1,6] naphthyridine as a π-bridge. *Dyes Pigment.* **164**, 188-97; 10.1039/C7CP02530K.

Balraju, P., Kumar, M., Roy, M.S., Sharma, G.D., 2009. Dye sensitized solar cells (DSSCs) based on modified iron phthalocyanine nanostructured TiO2 electrode and PEDOT: PSS counter electrode. *Synth.* Met. 159, 1325–1331. https://doi.org/10.1016/j.synthmet.2009.03.001.

Barjasteh-Askari, F., Davoudi, M., Dolatabadi, M., Ahmadzadeh, S., 2021. Iron-modified activated carbon derived from agro-waste for enhanced dye removal from aqueous solutions. Heliyon. 7 (6) https://doi.org/10.1016/j.heliyon.2021.e07191.

Britel, O., Fitri, A., Benjelloun, A. T., Slimi, A., Benzakour, M., McHarfi, M., 2022 Theoretical design of new carbazole based organic dyes for DSSCs applications. A DFT/TD-DFT insight, *J. Photochem. Photobiol. A-Chem.* **429**, 113902; 10.1016/j.jphotochem.2022.113902.

Bronskaya V., Manuyko G., Balzamov D., Ignashina T., Bashkirov D., Kharitonova O., Kondrateva, M., Khabibullina G., 2023. Copolymerization of butadiene and styrene under the influence of n-butyllithium. Arab. J. Chem. **16(11)**, 105205; 10.1016/j.arabjc.2023.105205.

Chen, C. C., Vinh Son, N., Chiu, H. C., Chen, Y. D., Wei, T. C., Yeh, C. Y., 2022. Anthracene-Bridged Sensitizers for Dye-Sensitized Solar Cells with 37% Efficiency under Dim Light. *Adv. Energy Mater.* **12**, 2104051; 10.1002/aenm.202104051.

Choudhary, N., Bee, S., Gupta, A., Tandon, P., 2013. Comparative vibrational spectroscopic studies, HOMO–LUMO and NBO analysis of N-(phenyl)-2,2-dichloroacetamide, N-(2-chloro phenyl)-2,2-dichloroacetamide and N-(4-chloro phenyl)-2,2-dichloroacetamide based on density functional theory. Comput. Theor. Chem. 1016, 8–21. https://doi.org/10.1016/j.molstruc.2011.07.022.

Cui, L., Zhou, J., Zhang, Y., Meng, X., Wang, H., Liu, B., 2023. Molecular engineering of auxiliary acceptor for the development of efficient organic D-A-π-A sensitizers. *Dyes Pigment.* **216**, 111322; 10.1016/j.dyepig.2023.111322.

Delgado-Montiel, T., Baldenebro-Lopez, J., Soto-Rojo, R., Glossman-Mitnik, D., 2020, Theoretical Study of the Effect of π-Bridge on Optical and Electronic Properties of Carbazole-Based Sensitizers for DSSCs, *Molecules.* **25**, 3670; 10.1016/j.molstruc.2011.07.022.

Dell'Orto, E., Raimondo, L., Sassella, A., Abbotto, A., 2012. Dye-sensitized solar cells: spectroscopic evaluation of dye loading on TiO_2. J. Mater. Chem. 22, 11364–11369. https://doi.org/10.1039/C2JM30481C.

Dolatabadi, M., Naidu, H., Ahmadzadeh, S., 2021. A green approach to remove acetamiprid insecticide using pistachio shell-based modified activated carbon; economical groundwater treatment. J. Clean. Prod. 316, 128226 https://doi.org/10.1016/j.jclepro.2021.128226.

Dolatabadi, M., Naidu, H., Ahmadzadeh, S., 2022a. Adsorption characteristics in the removal of chlorpyrifos from groundwater using magnetic graphene oxide and carboxy methyl cellulose composite. Sep. Purif. Technol. 300, 121919 https://doi.org/10.1016/j.seppur.2022.121919.

Dolatabadi, M., Kheirieh, A., Yoosefian, M., Ahmadzadeh, S., 2022b. Hydroxyzine removal from the polluted aqueous solution using the hybrid treatment process of electrocoagulation and adsorption; optimization, and modeling. Appl Water Sci 12 (11), 254. https://doi.org/10.1007/s13201-022-01780-7.

Duvva, N., Eom, Y. K., Reddy, G., Schanze, K. S., Giribabu, L., 2020. Bulky Phenanthroimidazole-Phenothiazine D-π-A Based Organic Sensitizers for Application in Efficient Dye-Sensitized Solar Cells. *ACS Appl. Energy Mater.* **3**, 6758-67; 10.1021/acsaem.0c00892.

Elkabous, M., Karzazi, Y., 2024. Theoretical study of new 3-(methylthio)-8-phenyl-8H-thieno [2, 3-b] indole derivatives for application in DSSC: Solvent effect, adsorption process on the surface of TiO2. Arab. J. Chem. 17 (1), 105457 https://doi.org/10.1016/j.arabjc.2023.105457.

Elmorsy, M. R., Badawy, S. A., Abdel-Latif, E., Assiri, M. A., Ali, T. E., 2023. Significant improvement of dye-sensitized solar cell performance using low-band-gap chromophores based on triphenylamine and carbazole as donors. *Dyes Pigment.* **214**, 111206; 10.1016/j.dyepig.2023.111206.

Ethirajan, M., Joshi, P., William III, W.H., Ohkubo, K., Fukuzumi, S., Pandey, R.K., 2011. Remarkable Regioselective Position-10 Bromination of Bacteriopyropheophorbide-a and Ring-B Reduced Pyropheophorbide-a. Org. Lett. 13, 1956–1959. https://doi.org/10.1021/ol200314v.

Frisch MJ, Trucks GW, Schlegel HB, Scuseria GE, Robb MA, Cheeseman JR, Scalmani G, Barone V, Mennucci B, Petersson GA, Nakatsuji H, Caricato M, Li X, Hratchian H P, Izmaylov A F, Bloino J, Zheng G, Sonnenberg JL, Hada M, Ehara M, Toyota K, Fukuda R, Hasegawa J, Ishida M, Nakajima T, Honda Y, Kitao O, Nakai H, Vreven T, Montgomery Jr JA, Peralta JE, Ogliaro F, Bearpark MJ, Heyd J, Brothers EN, Kudin KN, Staroverov VN, Kobayashi R, Normand J, Raghavachari K, Rendell AP, Burant JC, Iyengar SS, Tomasi J, Cossi M, Rega N, Millam NJ, Klene M, Knox JE, Cross JB, Bakken V, Adamo C, Jaramillo J, Gomperts R, Stratmann RE, Yazyev O, Austin AJ, Cammi R, Pomelli C, Ochterski JW, Martin RL, Morokuma K, Zakrzewski VG, Voth GA, Salvador P, Dannenberg JJ, Dapprich S, Daniels AD, Farkas Ö, Foresman JB, Cioslowski J, Fox DJ. *Gaussian 09*, Gaussian, Inc: Wallingford, CT, USA, **2009**.

Gao, F., Yang, C.L., Wang, M.S., Ma, X.G., Yi, Y.G., 2019. Theoretical insight on the nanocomposite of tetraphenylporphyrin-graphene oxide quantum dot as a sensitizer of DSSC. J. Photochem. Photobiol. A-Chem. 379, 24–31. https://doi.org/10.1016/j.jphotochem.2019.05.002.

Grifoni, F., Bonomo, M., Naim, W., Barbero, N., Alnasser, T., Dzeba, I., Giordano, M., Tsaturyan, A., Urbani, M., Torres, T., Barolo, C., Sauvage., F., 2021. Toward Sustainable, Colorless, and Transparent Photovoltaics: State of the Art and Perspectives for the Development of Selective Near-Infrared Dye-Sensitized Solar Cells. *Adv. Energy Mater.* **11**, 2101598; 10.1002/aenm.202101598.

Hachi, M., Slimi, A., Fitri, A., Benjelloun, A. T., El khattabi, S., Benzakour, M., McHarfi, M., Khenfouch, M., Zorkani, I., Bouachrine, M., 2021. Theoretical design and characterization of D-A_1-A based organic dyes for efficient DSSC by altering promising acceptor (A_1) moiety. *J. Photochem. Photobiol. A.* **407**, 113048; 10.1016/j.jphotochem.2020.113048.

Housecroft, C.E., Constable, E.C., 2022. Solar energy conversion using first row d-block metal coordination compound sensitizers and redox mediators. Chem. Sci. 13, 1225–1262. https://doi.org/10.1039/D1SC06828H.

Huang, Y., Zhou, W., Li, X., Jiang, L., Song, Y., 2021. Highly broadband NLO response of acceptor–donor–acceptor materials with a planar conformation. Mater. Adv. 2, 2097–2103. https://doi.org/10.1039/D0MA00918K.

Huaulme, Q., Mwalukuku, V.M., Joly, D., Liotier, J., Kervella, Y., Maldivi, P., Narbey, S., Oswald, F., Riquelme, A.J., Anta, J.A., Demadrille, R., 2020. Photochromic dye-sensitized solar cells with light-driven adjustable optical transmission and power conversion efficiency. Nat. Energy 5, 468–477. https://doi.org/10.1038/s41560-020-0624-7.

Johnson, E.R., Keinan, S., Mori-Sánchez, P., Contreras-García, J., Cohen, A.J., Yang, W., 2010. Revealing Noncovalent Interactions. J. Am. Chem. Soc. 132, 6498–6506. https://doi.org/10.1021/ja100936w.

Kabir, F., Sakib, S.N., 2019. Various impacts of blocking layer on the cell stability in natural dye based dye-synthesized solar cell. Optik 180, 684–690. https://doi.org/10.1016/j.ijleo.2018.11.142.

Kharkwal, D., Sharma, N., Kumar Gupta, S., Mohan Singh Negi, C., 2021. Enhanced performance of dye-sensitized solar cells by co-sensitization of metal-complex and organic dye. Sol. Energy 230, 1133–1140. https://doi.org/10.1016/j.solener.2021.11.037.

Koeppe, R., Bossart, O., Calzaferri, G., Sariciftci, N. S., 2007. Advanced photon-harvesting concepts for low-energy gap organic solar cells. *Solar Energy Materials and Solar Cells*. **91**, 986-95; 10.1016/j.solmat.2007.01.008.

Lazrak, M., Toufik, H., Bouzzine, S.M., Bih, H., Lamchouri, F., 2018. The computational study of bridge effect in D-π-A photosensitive dyes, based on triphenylamine. IOP Conf. Ser.: Earth Environ. Sci. 161, 012021 https://doi.org/10.1088/1755-1315/161/1/012021.

Le Bahers, T., Pauporte, T., Scalmani, G., Adamo, C., Ciofini, I., 2009. A TD-DFT investigation of ground and excited state properties in indoline dyes used for dye-sensitized solar cells. PCCP 11, 11276–11284. https://doi.org/10.1039/B914626A.

Lee, H.M., Yoon, J.H., 2018. Power performance analysis of a transparent DSSC BIPV window based on 2 year measurement data in a full-scale mock-up. Appl. Energy 225, 1013–1021. https://doi.org/10.1016/J.APENERGY.2018.04.086.

Li, X., Aftab, S., Hussain, S., Kabir, F., Henaish, A.M.A., Al-Sehemi, A.G., 2024a. Dimensional diversity (0D, 1D, 2D, 3D) in Perovskite solar cells: Exploring the potential of mix-dimensional integrations. J. Mater. Chem. A. https://doi.org/10.1039/D3TA06953B.

Li, S., Chen, J., He, X., Zheng, Y., Yu, C., Lu, H., 2023. Comparative study of the micro-mechanism of charge redistribution at metal-semiconductor and semimetal-semiconductor interfaces: Pt (Ni)-MoS2 and Bi-MoS2 (WSe2) as the prototype. Appl. Surf. Sci. 623, 157036 https://doi.org/10.1016/j.apsusc.2023.157036.

Li, Y.C., Li, X., Xu, Y.L., 2021. Theoretical screening of high-efficiency sensitizers with D-π-A framework for DSSCs by altering promising donor group. Sol. Energy 196, 146–156. https://doi.org/10.1016/j.solener.2019.11.092.

Li, W., Wang, J., Chen, J., Bai, F.Q., Zhang, H.X., 2014. Theoretical investigation and design of high-efficiency dithiafulvenyl-based sensitizers for dye-sensitized solar cells: the impacts of elongating π-spacers and rigidifying dithiophene. PCCP 16, 9458–9468. https://doi.org/10.1039/C4CP00968A.

Li, H., Wu, Y., Xu, Z., Wang, Y., 2024b. In situ anchoring Cu nanoclusters on Cu-MOF: A new strategy for a combination of catalysis and fluorescence toward the detection of

H_2O_2 and 2, 4-DNP. Chem. Eng. J. 479, 147508 https://doi.org/10.1016/j.cej.2023.147508.
Litani-Barzilai, I., Bulatov, V., Gridin, V.V., Schechter, I., 2004. Detector based on time-resolved ion-induced voltage in laser multiphoton ionization and laser-induced fluorescence. Anal. Chim. Acta 501, 151–156. https://doi.org/10.1016/j.aca.2003.09.025.
Liu, Z., Lu, T., Chen, Q., 2020. An sp-hybridized all-carboatomic ring, cyclo[18]carbon: Electronic structure, electronic spectrum, and optical nonlinearity. Carbon 165, 461–467. https://doi.org/10.1016/j.carbon.2020.05.023.
Lu, T., Chen, F., 2012. Multiwfn: A multifunctional wavefunction analyzer. J. Comput. Chem. 33, 580–592. https://doi.org/10.1002/jcc.22885.
Lu, T., Chen, F., 2013. Revealing the nature of intermolecular interaction and configurational preference of the nonpolar molecular dimers (H2)2, (N2)2, and (H2)(N2). J. Mol. Model. 19, 5387–5395. https://doi.org/10.1007/s00894-013-2034-2.
Lu, T., Chen, Q., 2021. Interaction Region Indicator (IRI): A Very Simple Real Space Function Clearly Revealing Both Chemical Bonds and Weak Interactions. Chemistry-Methods. 1, 231–239. https://doi.org/10.1002/cmtd.202100007.
Lu, T., Chen, Q., 2023. Simple, efficient, and universal energy decomposition analysis method based on dispersion-corrected density functional theory. Chem. A Eur. J. 127, 7023–7035. https://doi.org/10.1021/acs.jpca.3c04374.
Ma, W., Jiao, Y., Meng, S., 2014. Predicting energy conversion efficiency of dye solar cells from first principles. J. Phys. Chem. C 118, 16447–16457. https://doi.org/10.1021/jp410982e.
Marenich, A.V., Cramer, C.J., Truhlar, D.G., 2009. Universal solvation model based on solute electron density and on a continuum model of the solvent defined by the bulk dielectric constant and atomic surface tensions. J. Phys. Chem. B 113, 6378–6396. https://doi.org/10.1021/jp810292n.
Meenakshi, R., 2017. Spectral investigations DFT based global reactivity descriptors, Inhibition efficiency and analysis of 5-chloro-2-nitroanisole as π-spacer with donor-acceptor variations effect for DSSCs performance. J. Mol. Struct. 1127, 694–707. https://doi.org/10.1016/j.molstruc.2016.08.030.
Meti, P., Nagaraju, G., Yang, J. W., Jung, S. H., Gong, Y. D., 2019. Synthesis of dipyrrolopyrazine-based sensitizers with a new π-bridge end-capped donor-acceptor framework for DSSCs: a combined experimental and theoretical investigation. *New J. Chem.* **43**, 3017-25; 10.1039/C8NJ06083E.
Murray, J. S., Politzer, P., 2011. The electrostatic potential: an overview. *Wiley Interdiscip. Rev.-Comput. Mol. Sci.* **1**, 153-63; 10.1002/wcms.19.
Nachimuthu, S., Chen, W.C., Leggesse, E.G., Jiang, J.C., 2016. First principles study of organic sensitizers for dye sensitized solar cells: effects of anchoring groups on optoelectronic properties and dye aggregation. PCCP 18, 1071–1081. https://doi.org/10.1039/C5CP04877J.
Nagarajan, B., Kushwaha, S., Elumalai, R., Mandal, S., Ramanujam, K., Raghavachari, D., 2017. Novel ethynyl-pyrene substituted phenothiazine based metal free organic dyes in DSSC with 12% conversion efficiency. J. Mater. Chem. A 5, 10289–10300. https://doi.org/10.1039/D4TA90044H.
Noh, H.J., Ji, J.M., Hwang, S.P., Kim, C.H., Kim, H.K., 2021. D-π-A-structured organic sensitizers with π-extended auxiliary acceptor units for high-performance dye-sensitized solar cells. Dyes Pigment. 195, 109681 https://doi.org/10.1016/j.dyepig.2021.109681.
O'Regan, B., Grätzel, M., 1991. A low-cost, high-efficiency solar cell based on dye-sensitized colloidal TiO_2 films. Nature 353, 737–740. https://doi.org/10.1038/353737a0.
Parr, R.G., Donnelly, R.A., Levy, M., Palke, W.E., 1978. Electronegativity: The density functional viewpoint. J. Chem. Phys. 68, 3801–3807. https://doi.org/10.1063/1.436185.
Patil, D.S., Avhad, K.C., Sekar, N., 2018. Linear correlation between DSSC efficiency, intramolecular charge transfer characteristics, and NLO properties - DFT approach. Comput. Theor. Chem. 1138, 75–83. https://doi.org/10.1016/j.comptc.2018.06.006.
Pelzer, K.M., Darlin, S.B., 2016. Charge generation in organic photovoltaics: a review of theory and computation. Mol. Syst. Des. Eng. 1, 10–24. https://doi.org/10.1039/C6ME00005C.
Pounraj, P., Mohankumar, V., Pandian, M.S., Ramasamy, P., 2018. Donor functionalized quinoline based organic sensitizers for dye sensitized solar cell (DSSC) applications: DFT and TD-DFT investigations. J. Mol. Model. 24, 1–23. https://doi.org/10.1007/s00894-018-3872-8.
Prakash, K., Alsaleh, A.Z., Rathi, P., Sharma, A., Sankar, M., D'Souza, F., 2019. Synthesis, spectral, electrochemical and photovoltaic studies of A_3B porphyrinic dyes having peripheral donors. ChemPhysChem 20, 2627–2634. https://doi.org/10.1002/cphc.201900604.
Preat, J., Jacquemin, D., Perpete, E. A., 2010. Towards new efficient dye-sensitised solar cells. *Energy Environ. Sci.* **3**, 891-904; 10.1039/C000474J.
Quang, L. N. D., Kaliamurthy, A. K., Hao, N. H., 2021. Co-sensitization of metal based N719 and metal free D35 dyes: An effective strategy to improve the performance of DSSC. *Optical Materials.* **111**, 110589; 10.1016/j.optmat.2020.110589.
Ramesh, K., Gnanavel., B., 2021. Fabrication and characterization of RGO/WO3 nanocomposites based working electrode for dye-sensitized solar cells (DSSCs). *Mater. Today: Proc.* **157**, 112047; 10.1016/j.matpr.2021.04.023.
Ren, H., Li, X., 2013. Quantum chemistry theoretical investigation on the dissociation constant of 2-thioxanthine acid, *Computers and Applied Chemistry*. **30**, 553-6; 10.1021/acs.jcim.2c01468.
Roy, J.K., Kar, S., Leszczynski, J., 2019. Optoelectronic properties of C_{60} and C_{70} fullerene derivatives: designing and evaluating novel candidates for efficient P3HT polymer solar cells. Materials. 12, 2282 https://doi.org/10.3390/ma12142282.
Runge, E., Gross, E. K. U., 1984. Density-Functional Theory for Time-Dependent Systems. Physical Review Letters. 52(12), 997-1000; 10.1103/PhysRevLett.52.997.
Saji, V.S., Pyo, M., 2010. Effect of coadsorbents on DSSC sensitized by NIR absorbing poly(ethyl thieno[3,4-b]thiophene-2-carboxylate). Curr. Appl Phys. 10, S410–S413. https://doi.org/10.1016/j.cap.2010.02.011.
Sen, A., Groβ, A., 2020. Effect of Electron-Withdrawing/-Donating Groups on the Sensitizing Action of the Novel Organic Dye "3-(5-(4-(Diphenylamino)styryl) thiophen-2-yl)-2-cyanoacrylic Acid" for N-Type Dye-Sensitized Solar Cells: A Theoretical Study. *J. Phys. Chem. C* **124**, 8526-40; 10.1021/acs.jpcc.0c00369.
Senge, M. O., Fazekas, M., Notaras, E. G. A., Blau, W. J., Zawadzka, M., Locos, O. B., Mhuircheartaigh, E. M. N., 2007. Nonlinear optical properties of porphyrins. *Adv. Mater.* **19**, 2737-74; 2007 10.1002/adma.200601850.
Sharma, K., Sharma, V., Sharma, S.S., 2018. Dye-sensitized solar cells: fundamentals and current status. Nanoscale Res Lett. 13, 1–46. https://doi.org/10.1186/s11671-018-2760-6.
Singh, M., Kanaparthi, R.K., 2022. Theoretical exploration of 1,3-Indanedione as electron acceptor-cum-anchoring group for designing sensitizers towards DSSC applications. Sol. Energy 237, 456–469. https://doi.org/10.1016/j.solener.2022.01.018.
Sultan, U., Ahmadloo, F., Cha, G., Goekcan, B., Hejazi, S., Yoo, J.-E., Nhat Truong, N., Altomare, M., Schmuki, P., Killian, M. S., 2020. A High-Field Anodic NiO Nanosponge with Tunable Thickness for Application in p-Type Dye-Sensitized Solar Cells. *ACS Appl. Energy Mater.* **3**, 7865-72; 10.1021/acsaem.0c01249.
Sun, D., Yang, C., Liu, T., Li, Y., 2023. Photoelectric Performance of Several Dithienoheterocycles Dyes and Nanocomposite of Dyes/Graphene Quantum Dots for DSSCs. *Adv. Theory Simul.* **6**, 2200940; 10.1002/adts.202200940.
Sun, Y., Sun, Y., Dall'Agnese, C., Wang, X.F., Chen, G., Kitao, O., Tamiaki, H., Sakai, K., Ikeuchi, T., Sasaki, S.I., 2018. Dyad sensitizer of chlorophyll with indoline dye for panchromatic photocatalytic hydrogen evolution. ACS Appl. Energ. Mater. 1 (6), 2813–2820. https://doi.org/10.1021/acsaem.8b00380.
Suramitr, S., Piriyagagoon, A., Wolschann, P., Hannongbua, S., 2012. Theoretical study on the structures and electronic properties of oligo(p-phenylenevinylene) carboxylic acid and its derivatives: effects of spacer and anchor groups. Theor. Chem. Acc. 131, 1–15. https://doi.org/10.1007/s00214-012-1209-8.
Tamiaki, H., Kunieda, M., 2011. 51 photochemistry of chlorophylls and their synthetic analogs. Handb. Porphyry. Sci. 11, 223–290. https://doi.org/10.1142/9789814322386_0003.
Tong, J., Huang, Y., Liu, W., Shou, M., An, L., Jiang, X., Guo, P., Han, Y., Liang, Z., Li, J., Xia, Y., 2022. Optimized molecular aggregation and photophysical process synergistically promoted photovoltaic performance in low-regularity benzo [c][1,2,5] thiadiazole-based medium-bandgap copolymers via modulating π bridges. J. Mater. Chem. C 10, 16028–16039. https://doi.org/10.1039/D2TC02786K.
Ullah, H., 2017. Inter-molecular interaction in Polypyrrole/TiO_2: A DFT study. J. Alloy. Compd. 692, 140–148. https://doi.org/10.1016/j.jallcom.2016.08.169.
Wang, Z., Fu, W., Hu, L., Zhao, M., Guo, T., Hrynsphan, D., Chen, J., 2021. Improvement of electron transfer efficiency during denitrification process by Fe-Pd/multi-walled carbon nanotubes: Possessed redox characteristics and secreted endogenous electron mediator. Sci. Total Environ. 781, 146686 https://doi.org/10.1016/j.scitotenv.2021.146686.
Wazzan, N., 2022. Theoretical investigation of anthanthrene-based dyes in dye-sensitized solar cell applications: Effect of nature of alkyl-substitutions and number of anchoring groups. Arab. J. Chem. 15 (8), 103969 https://doi.org/10.1016/j.arabjc.2022.103969.
Wu, H., Zhang, J., Ren, Y., Zhang, Y., Yuan, Y., Shen, Z., Li, S., Wang, P., 2020. Tuning the Color Palette of Semi-Transparent Solar Cells via Lateral π-Extension of Polycyclic Heteroaromatics of Donor-Acceptor Dyes. *ACS Appl. Energy Mater.* **3**, 4549-58; 10.1021/acsaem.0c00216.
Wuerthner, F., Kaiser, T.E., Saha-Moeller, C.R., 2011. J-Aggregates: From Serendipitous Discovery to Supramolecular Engineering of Functional Dye Materials. Angew. Chem.-Int. Edit. 50, 3376–3410. https://doi.org/10.1002/anie.201002307.
Yang, C., Song, P., Ma, F., Li, Y, 2023. Enhanced Photovoltaic Property and Panchromatic Photocatalytic by Forming D-p-A-Bacteriochlorin Dyads: A Computational Investigation. *Sol. RRL.* **7**, 2300106; 10.1002/solr.202300106.
Yang, C., Liu, T., Song, P., Ma, F., Li, Y., 2022. Revealing the photoelectric performance and multistep electron transfer mechanism in D-A-π-A dyes coupled with a chlorophyll derivative for co-sensitized solar cells. J. Mol. Liq. 368, 120797 https://doi.org/10.1016/j.molliq.2022.120797.
Ye, J. X., Li, N., Wang, X. F., Fujii, R., Yamano, Y., Sasaki, S. I., 2022. Enhancement of power conversion efficiency by chlorophyll and carotenoid co-sensitization in the biosolar cells. *J. Photochem. Photobiol. A-Chem.* **431**, 114042; 10.1016/j.jphotochem.2022.114042.
Zang, Z., Ma, F., Song, P., Li, Y., 2024. Enhanced Charge Separation and Short-Circuit Current by Doping with Chlorophyll in Cascaded Ternary Solar Cells. Acs Applied Energy Materials. **7(6)**, 2362-77; 10.1021/acsaem.3c03097.
Zang, Z., Yu, Y., Song, P., Ma, F., Li, Y., 2023. Nonfused dimethoxybenzene electron acceptors in organic solar cells: from molecular design to structure-performance relationship. J. Phys. Chem. C 127 (1), 110–124. https://doi.org/10.1021/acs.jpcc.2c07730.
Zhang, H., Chen, Z.E., Tian, H.R., 2020a. Molecular engineering of metal-free organic sensitizers with polycyclic benzenoid hydrocarbon donor for DSSC applications: The effect of the conjugate mode. Sol. Energy 198, 239–246. https://doi.org/10.1016/j.solener.2020.01.067.
Zhang, F., Jiang, K.J., Huang, J.H., Yu, C.C., Li, S.G., Chen, M.G., Yang, L.M., Song, Y.L., 2013. A novel compact DPP dye with enhanced light harvesting and charge transfer properties for highly efficient DSCs. J. Mater. Chem. A 1, 4858–4863. https://doi.org/10.1039/C3TA10618G.
Zhang, J., Kan, Y.H., Li, H.B., Geng, Y., Wu, Y., Su, Z.M., 2012. How to design proper π-spacer order of the D-π-A dyes for DSSCs? A density functional response. Dyes Pigment. 95 (313–21) https://doi.org/10.1016/j.dyepig.2012.05.020.

Zhang, G., Musgrave, C.B., 2007. Comparison of DFT methods for molecular orbital eigenvalue calculations. Chem. A Eur. J. 111, 1554–1561. https://doi.org/10.1021/jp061633o.

Zhang, D., Stojanovic, M., Ren, Y.M., Cao, Y.M., Eickemeyer, F.T., Socie, E., Vlachopoulos, N., Moser, J.E., Zakeeruddin, S.M., Hagfeldt, A., Grätzel, M., 2021. A molecular photosensitizer achieves a Voc of 1.24V enabling highly efficient and stable dye-sensitized solar cells with copper(II/I)-based electrolyte. Nat. Commun. 12, 1777. https://doi.org/10.1038/s41467-021-21945-3.

Zhang, J., Wang, L., Zhong, A., Huang, G., Wu, F., Li, D., Han, D., 2019. Deep red PhOLED from dimeric salophen Platinum (II) complexes. Dyes Pigments 162, 590–598. https://doi.org/10.1016/j.dyepig.2018.10.053.

Zhang, J., Zhong, A., Huang, G., Yang, M., Li, D., Teng, M., Han, D., 2020b. Enhanced efficiency with CDCA co-adsorption for dye-sensitized solar cells based on metallosalophen complexes. Sol. Energy 209, 316–324. https://doi.org/10.1016/j.solener.2020.08.096.

Zhao, G., Yang, Y., Zhang, C., Song, Y., Li, Y., 2021. The theoretical study of excited-state intramolecular proton transfer of N, N,-bis (salicylidene)-(2-(3′4′-diaminophenyl) benzothiazole). *J. Lumines.* **230**, 117741; 10.1016/j.jlumin.2020.117741.

Zhou, H., Ji, J.-M., Lee, H.S., Aftabuzzaman, M., Lee, D.-N., Kim, C.H., Kim, H.K., 2023. D-π-A Structured Porphyrin and Organic Dyes with Easily Synthesizable Donor Units for Low-Cost and Efficient Dye-Sensitized Solar Cells. ACS Appl Mater. Interfaces. 15, 39426–39434. https://doi.org/10.1021/acsami.3c08877.